FINAL REPORT

Graduate Studeny Research Program
(NGT-1-52114)

FLOWFIELD-DEPENDENT MIXED EXPLICIT-IMPLICIT (FDMEL) ALGORITHM FOR COMPUTATIONAL FLUID DYNAMICS

S. M. Garcia and T. J. Chung
Department of Mechanical and Aerospace Engineering
The University of Alabama in Huntsville
Huntsville, AL 35899

Submitted to

National Aeronautic and Space Administration
Langley Research Center
Hampton, VAA 23681-0001

June, 1997

FLOWFIELD-DEPENDENT MIXED EXPLICIT-IMPLICIT (FDMEI) ALGORITHM FOR COMPUTATIONAL FLUID DYNAMICS

S. M. Garcia and T. J. Chung
Department of Mechanical and Aerospace Engineering
The University of Alabama in Huntsville
Huntsville, AL 35899

ABSTRACT

Despite significant achievements in computational fluid dynamics, there still remain many fluid flow phenomena not well understood. For example, the prediction of temperature distributions is inaccurate when temperature gradients are high, particularly in shock wave turbulent boundary layer interactions close to the wall. Complexities of fluid flow phenomena include transition to turbulence, relaminarization, separated flows, transition between viscous and inviscid, incompressible and compressible flows, among others, in all speed regimes. The purpose of this paper is to introduce a new approach, called the **Flowfield-Dependent Mixed Explicit-Implicit (FDMEI)** method, in an attempt to resolve these difficult issues in CFD. In this process, a total of six implicitness parameters characteristic of the current flowfield are introduced. They are calculated from the current flowfield or changes of Mach numbers, Reynolds numbers, Peclet numbers, and Damköhler numbers (if reacting) at each nodal point and time step. This implies that every nodal point or element is provided with different or unique numerical scheme according to their current flowfield situations, whether compressible, incompressible, viscous, inviscid, laminar, turbulent, reacting, or nonreacting. In this procedure, discontinuities or fluctuations of all variables between adjacent nodal points are determined accurately. If these implicitness parameters are fixed to certain numbers instead of being calculated from the flowfield information, then practically all currently available schemes of finite differences or finite elements arise as special cases. Some benchmark problems to be presented in this paper will show the validity, accuracy, and efficiency of the proposed methodology.

1. INTRODUCTION

Nearly half a century has elapsed since the digital computer revolutionized computational technologies in engineering and mathematical physics. During this time finite difference methods (FDM) have dominated the field of computational fluid dynamics (CFD) [1-7], whereas the opposite is true for finite element methods (FEM) in solid mechanics. In recent years, however, the trend toward finite element methods in CFD appears to be increasingly favorable [8-14].

In general, the analyst preoccupied with the methods of his choice based on his educational background or research experience is seldom motivated to investigate other options. Thus, today the gap between these two disciplines is widely apart, despite the fact that the thorough understanding of the relations between FDM and FEM is beneficial. The purpose of this paper is an attempt to call for a new approach in which both FEM and FDM can be united toward the common goal of achieving the highest level of accuracy and efficiency in CFD. Similarities and dissimilarities must be identified in order to recognize merits and demerits of each method and to enable the analysts to choose the most desirable approach suitable for the particular task at hand.

One of the most important questions in CFD is how to deal with large gradients of the variable (density, velocity, pressure, temperature, and source terms). Rapid changes of Mach numbers, Reynolds numbers, Peclet numbers, and Damköhler numbers (if reacting) between adjacent nodal points or elements can be a crucial factor in determining whether the chosen computational scheme will succeed or fail. Furthermore, proper treatments for incompressibility and compressibility, viscous and inviscid flows, subsonic and supersonic flows, laminar and turbulent flows, nonreacting and reacting flows are extremely important. The most general case of fluid dynamics where these various flow properties may be depicted in external and internal hypersonic flows is shown in Fig 1a,b. A typical reacting flow (hydrogen-air reaction) can also be seen in Fig. 1c.

Can a single formulation and computer code be made available to satisfy all the requirements mentioned above? Can a single mathematical formulation lead to most of the currently available computational schemes both in FDM and FEM as special cases? Most importantly, will such an approach guarantee accuracy and efficiency? In this paper, we respond to these questions positively, based on the results obtained through example problems.

Toward this goal, our approach is based on the following procedure [15, 16], known as the Flowfield-Dependent Mixed Explicit-Implicit (FDMEI) scheme:

(a) Write the Navier-Stokes system of equations in a conservation form.

(b) Expand the conservation variable $\mathbf{U}^{n+1}$ in Taylor series up to and including the second-order time derivatives of the conservation variables.

(c) Introduce in step (b) six different flowfield-dependent implicitness parameters which are calculated from the changes in Mach numbers, Reynolds numbers, Peclet numbers, and Damköhler numbers (if reacting) between nodal points or local elements.

(d) Substitute step (a) and (c) into step (b) to obtain the increments of the conservation variables $\Delta \mathbf{U}^{n+1}$. As a result, the final form resembles the implicit factored scheme of Beam and Warming [1], but much more rigorous.

(e) Step (d) may be used either in FDM or FEM.

The computational procedure as described above is capable of resolving complex properties of fluid flows in general with shock waves, turbulence, and reacting flows in particular.

(1) Incompressible flows are dependent on changes in Reynolds number between nodal points in FDM and within local elements in FEM. Incompressibility conditions are characterized by these changes in Reynolds number.

(2) Compressible flows are dependent on changes in both Mach number and Reynolds number between nodal points in FDM and within local elements in FEM. Dilatational dissipation is characterized by these changes in Mach number and Reynolds number.

(3) Shock waves in compressible flows are dependent on changes in Mach number between nodal points in FDM and within local elements in FEM. Shock wave discontinuities are characterized by these changes in Mach number.

(4) High temperature gradient flows are dependent on changes in Peclet number between nodal points in FDM and within local elements in FEM. The convection vs diffusion in heat transfer is characterized by these changes in Peclet number.

(5) Reacting flows are dependent on changes in Damköhler number between nodal points in FDM and within local elements in FEM. The mass source vs convective transfer, mass source vs diffusive transfer, heat source vs convective heat transfer, heat source vs conductive heat transfer, and heat source vs diffusive heat transfer are characterized by these changes in Damköhler number.

(6) Direct numerical simulation (DNS) for turbulent flows in which mesh refinements are carried out until turbulence length microscales are resolved without turbulence models can not be reliable particularly for high speed compressible turbulent flows unless the computational scheme is capable of treating high gradients of variables as described in (2) above. To improve turbulence calculations, Legendre polynomial spectral modes may be added as shown in [15]. Whether or not the spectral mode approach is advantageous for an overall computational efficiency remains to be seen. Due to the limitation of computer time, the example problems in this paper are not intended for DNS microscale resolutions.

Details of the mathematical formulations as described above are presented in Section 2, implementation and computational process in Section 3, some example problems in Section 4, and concluding remarks in Section 5.

2. MATHEMATICAL FORMULATIONS

For the general purpose program considering the compressible viscous reacting flows, we write the conservation form of the Navier-Stokes system of equations as

$$\frac{\partial \mathbf{U}}{\partial t}+\frac{\partial \mathbf{F}_i}{\partial x_i}+\frac{\partial \mathbf{G}_i}{\partial x_i}=\mathbf{B} \tag{1}$$

where $\mathbf{U}$, $\mathbf{F}_i$, $\mathbf{G}_i$, and $\mathbf{B}$ denote the conservation flow variables, convection flux variables, diffusion flux variables, and source terms, respectively,

$$\mathbf{U}=\begin{bmatrix}\rho\\ \rho v_j\\ \rho E\\ \rho Y_k\end{bmatrix},\ \mathbf{F}_i=\begin{bmatrix}\rho v_i\\ \rho v_i v_j+p\delta_{ij}\\ \rho E v_i+p v_i\\ \rho Y_k v_i\end{bmatrix},\ \mathbf{G}_i=\begin{bmatrix}0\\ -\tau_{ij}\\ -\tau_{ij}v_j-kT_{,i}-\sum \rho c_{pk}TD_{km}Y_{k,i}\\ -\rho D_{km}Y_{k,i}\end{bmatrix},\ \mathbf{B}=\begin{bmatrix}0\\ \rho f_j\\ -H_k^o w_k+\rho f_j v_j\\ w_k\end{bmatrix}$$

where $f_j=\sum_{k=1}^{N} Y_k f_{kj}$ is the body force, Y_k is the chemical species, H_k^o is the zero-point enthalpy, w_k is the reaction rate, and D_{km} is the binary diffusivity. Additional equations for vibrational and electronic energies may be included in (1) for hypersonics.

Expanding the conservation variables $\mathbf{U}$ in Taylor series including the first and second derivatives, we have

$$\mathbf{U}^{n+1}=\mathbf{U}^n+\Delta t\frac{\partial \mathbf{U}^{n+s_1}}{\partial t}+\frac{\Delta t^2}{2}\frac{\partial^2 \mathbf{U}^{n+s_2}}{\partial t^2}+O\left(\Delta t^3\right) \tag{2}$$

where s_1 and s_2 are the implicitness parameters defined such that

$$\frac{\partial \mathbf{U}^{n+s_1}}{\partial t}=\frac{\partial \mathbf{U}^n}{\partial t}+s_1\frac{\partial \Delta \mathbf{U}^{n+1}}{\partial t} \qquad 0\le s_1\le 1 \tag{3}$$

$$\frac{\partial^2 \mathbf{U}^{n+s_2}}{\partial t^2}=\frac{\partial^2 \mathbf{U}^n}{\partial t^2}+s_2\frac{\partial^2 \Delta \mathbf{U}^{n+1}}{\partial t^2} \qquad 0\le s_2\le 1 \tag{4}$$

with $\Delta \mathbf{U}^{n+1}=\mathbf{U}^{n+1}-\mathbf{U}^n$. It is assumed that the convection flux $\mathbf{F}_i$ is a function of $\mathbf{U}$ and the diffusion flux $\mathbf{G}_i$ is a function of both $\mathbf{U}$ and its gradient $\mathbf{U}_{,i}$. Thus, we have

$$\frac{\partial \mathbf{U}}{\partial t}=-\frac{\partial \mathbf{F}_i}{\partial x_i}-\frac{\partial \mathbf{G}_i}{\partial x_i}+\mathbf{B} \tag{5}$$

$$\frac{\partial^2 \mathbf{U}}{\partial t^2}=-\frac{\partial}{\partial x_i}\left(\mathbf{a}_i\frac{\partial \mathbf{U}}{\partial t}\right)-\frac{\partial}{\partial x_i}\left(\mathbf{b}_i\frac{\partial \mathbf{U}}{\partial t}\right)-\frac{\partial^2}{\partial x_i\partial x_j}\left(\mathbf{c}_{ij}\frac{\partial \mathbf{U}}{\partial t}\right)+\mathbf{d}\left(\frac{\partial \mathbf{U}}{\partial t}\right) \tag{6}$$

where the convection Jacobian $\mathbf{a}_i$, the diffusion Jacobian $\mathbf{b}_i$, the diffusion gradient Jacobian $\mathbf{c}_{ij}$, and the source Jacobian $\mathbf{d}$ are defined as

$$\mathbf{a}_i = \frac{\partial \mathbf{F}_i}{\partial \mathbf{U}} \quad , \qquad \mathbf{b}_i = \frac{\partial \mathbf{G}_i}{\partial \mathbf{U}} \quad , \qquad \mathbf{c}_{ij} = \frac{\partial \mathbf{G}_i}{\partial \mathbf{U}_{,j}} \quad , \qquad \mathbf{d} = \frac{\partial \mathbf{B}}{\partial \mathbf{U}} \tag{7}$$

Substituting (3) - (6) into (2) and assuming the product of the diffusion gradient Jacobian with third order spatial derivatives to be negligible, we obtain

$$\begin{aligned}
\Delta \mathbf{U}^{n+1} = \Delta t & \left[-\frac{\partial \mathbf{F}_i^n}{\partial x_i} - \frac{\partial \mathbf{G}_i^n}{\partial x_i} + \mathbf{B}^n + s_1 \left(-\frac{\partial \Delta \mathbf{F}_i^{n+1}}{\partial x_i} - \frac{\partial \Delta \mathbf{G}_i^{n+1}}{\partial x_i} + \Delta \mathbf{B}^{n+1} \right) \right] \\
& + \frac{\Delta t^2}{2} \left\{ \left[\frac{\partial}{\partial x_i} (\mathbf{a}_i + \mathbf{b}_i) \left(\frac{\partial \mathbf{F}_j^n}{\partial x_j} + \frac{\partial \mathbf{G}_j^n}{\partial x_j} - \mathbf{B}^n \right) - \mathbf{d} \left(\frac{\partial \mathbf{F}_i^n}{\partial x_i} + \frac{\partial \mathbf{G}_i^n}{\partial x_i} - \mathbf{B}^n \right) \right] \right. \\
& + s_2 \left[\frac{\partial}{\partial x_i} (\mathbf{a}_i + \mathbf{b}_i) \left(\frac{\partial \Delta \mathbf{F}_j^{n+1}}{\partial x_j} + \frac{\partial \Delta \mathbf{G}_j^{n+1}}{\partial x_j} - \Delta \mathbf{B}^{n+1} \right) \right. \\
& \left. \left. - \mathbf{d} \left(\frac{\partial \Delta \mathbf{F}_i^{n+1}}{\partial x_i} + \frac{\partial \Delta \mathbf{G}_i^{n+1}}{\partial x_i} - \Delta \mathbf{B}^{n+1} \right) \right] \right\} + \mathrm{O}\left(\Delta t^3\right)
\end{aligned} \tag{8}$$

In order to provide different implicitness (different numerical treatments or schemes) to different physical quantities, we reassign s_1 and s_2 associated with the diffusion and source terms, respectively,

$$s_1 \Delta \mathbf{G}_i \Rightarrow s_3 \Delta \mathbf{G}_i \quad , \qquad s_1 \Delta \mathbf{B} \Rightarrow s_5 \Delta \mathbf{B} \tag{9a}$$

$$s_2 \Delta \mathbf{G}_i \Rightarrow s_4 \Delta \mathbf{G}_i \quad , \qquad s_2 \Delta \mathbf{B} \Rightarrow s_6 \Delta \mathbf{B} \tag{9b}$$

with the various implicitness parameters defined as

s_1 = first order convection implicitness parameter

s_2 = second order convection implicitness parameter

s_3 = first order diffusion implicitness parameter

s_4 = second order diffusion implicitness parameter

s_5 = first order source term implicitness parameter

s_6 = second order source term implicitness parameter

The first order implicitness parameters s_1, s_3, and s_5 will be shown to be flowfield dependent with the solution accuracy assured by taking into account the flowfield gradients, whereas the second order implicitness parameters s_2, s_4, and s_6, which are also flowfield dependent, mainly act as artificial viscosity, contributing to the solution stability.

Substituting these implicitness parameters as defined in (9) into (8), we obtain

$$\Delta\mathbf{U}^{n+1}+\Delta t\left[s_1\left(\frac{\partial\left(\mathbf{a}_i\Delta\mathbf{U}^{n+1}\right)}{\partial x_i}\right)+s_3\left(\frac{\partial\left(\mathbf{b}_i\Delta\mathbf{U}^{n+1}\right)}{\partial x_i}+\frac{\partial^2\left(\mathbf{c}_{ij}\Delta\mathbf{U}^{n+1}\right)}{\partial x_i\partial x_j}\right)-s_5\,\mathbf{d}\Delta\mathbf{U}^{n+1}\right]$$

$$-\frac{\Delta t^2}{2}\left\{s_2\left[\frac{\partial^2\left(\left(\mathbf{a}_i\mathbf{a}_j+\mathbf{b}_i\mathbf{a}_j\right)\Delta\mathbf{U}^{n+1}\right)}{\partial x_i\partial x_j}-\frac{\mathbf{d}\partial\left(\mathbf{a}_i\Delta\mathbf{U}^{n+1}\right)}{\partial x_i}\right]+s_4\left[\left(\frac{\partial^2\left(\left(\mathbf{a}_i\mathbf{b}_j+\mathbf{b}_i\mathbf{b}_j\right)\Delta\mathbf{U}^{n+1}\right)}{\partial x_i\partial x_j}\right)\right.\right.$$

$$\left.\left.-\mathbf{d}\left(\frac{\partial\left(\mathbf{b}_i\Delta\mathbf{U}^{n+1}\right)}{\partial x_i}+\frac{\partial^2\left(\mathbf{c}_{ij}\Delta\mathbf{U}^{n+1}\right)}{\partial x_i\partial x_j}\right)\right]-s_6\left[\mathbf{d}\frac{\partial\left(\left(\mathbf{a}_i+\mathbf{b}_i\right)\Delta\mathbf{U}^{n+1}\right)}{\partial x_i}-\mathbf{d}^2\,\Delta\mathbf{U}^{n+1}\right]\right\}+\Delta t\left(\frac{\partial\mathbf{F}_i^n}{\partial x_i}+\frac{\partial\mathbf{G}_i^n}{\partial x_i}-\mathbf{B}^n\right)$$

$$-\frac{\Delta t^2}{2}\left[\frac{\partial}{\partial x_i}\left(\left(\mathbf{a}_i+\mathbf{b}_i\right)\left(\frac{\partial\mathbf{F}_j^n}{\partial x_j}+\frac{\partial\mathbf{G}_j^n}{\partial x_j}-\mathbf{B}^n\right)\right)-\mathbf{d}\left(\frac{\partial\mathbf{F}_i^n}{\partial x_i}+\frac{\partial\mathbf{G}_i^n}{\partial x_i}-\mathbf{B}^n\right)\right]+O\left(\Delta t^3\right)=0 \tag{10}$$

with

$$\Delta\mathbf{B}^{n+1}=\frac{\partial\mathbf{B}}{\partial\mathbf{U}}\Delta\mathbf{U}^{n+1}=\mathbf{d}\Delta\mathbf{U}^{n+1} \tag{11}$$

For simplicity we may rearrange (10) in a compact form,

$$\mathbf{R}=\Delta\mathbf{U}^{n+1}+\frac{\partial}{\partial x_i}\left(\mathbf{E}_i\,\Delta\mathbf{U}^{n+1}\right)+\frac{\partial^2}{\partial x_i\partial x_j}\left(\mathbf{E}_{ij}\,\Delta\mathbf{U}^{n+1}\right)+\mathbf{Q}^n+O\left(\Delta t^3\right)=0 \tag{12}$$

or

$$\left(\mathbf{A}+\frac{\partial\mathbf{E}_i}{\partial x_i}+\frac{\partial^2\mathbf{E}_{ij}}{\partial x_i\partial x_j}\right)\Delta\mathbf{U}^{n+1}=-\mathbf{Q}^n \tag{13}$$

with

$$\mathbf{A}=\mathbf{I}-\Delta t\,s_5\,\mathbf{d}-\frac{\Delta t^2}{2}s_6\,\mathbf{d}^2 \tag{14}$$

$$\mathbf{E}_i=\Delta t\left(s_1\mathbf{a}_i+s_3\mathbf{b}_i\right)+\frac{\Delta t^2}{2}\left[s_6\,\mathbf{d}\left(\mathbf{a}_i+\mathbf{b}_i\right)+s_2\,\mathbf{d}\mathbf{a}_i+s_4\mathbf{d}\mathbf{b}_i\right] \tag{15}$$

$$\mathbf{E}_{ij}=\Delta t\,s_3\mathbf{c}_{ij}-\frac{\Delta t^2}{2}\left[s_2\left(\mathbf{a}_i\mathbf{a}_j+\mathbf{b}_i\mathbf{a}_j\right)+s_4\left(\mathbf{a}_i\mathbf{b}_j+\mathbf{b}_i\mathbf{b}_j-\mathbf{d}\mathbf{c}_{ij}\right)\right] \tag{16}$$

$$\mathbf{Q}^n = \frac{\partial}{\partial x_i}\left[\left(\Delta t + \frac{\Delta t^2}{2}\mathbf{d}\right)\left(\mathbf{F}_i^n + \mathbf{G}_i^n\right) + \frac{\Delta t^2}{2}\left(\mathbf{a}_i + \mathbf{b}_i\right)\mathbf{B}^n\right] - \frac{\partial^2}{\partial x_i \partial x_j}\left[\frac{\Delta t^2}{2}\left(\mathbf{a}_i + \mathbf{b}_i\right)\left(\mathbf{F}_j^n + \mathbf{G}_j^n\right)\right] - \left(\Delta t + \frac{\Delta t^2}{2}\mathbf{d}\right)\mathbf{B}^n \tag{17}$$

We may allow the source terms in the LHS of (13) to lag from the time step $n + 1$ to n, so that (13b) can be written as

$$\left(\mathbf{I} + \frac{\partial \mathbf{E}_i}{\partial x_i} + \frac{\partial^2 \mathbf{E}_{ij}}{\partial x_i \partial x_j}\right)\Delta \mathbf{U}^{n+1} = -\mathbf{Q}^n \tag{18}$$

with

$$\mathbf{Q}^n = \frac{\partial}{\partial x_i}\left[\left(\Delta t + \frac{\Delta t^2}{2}\mathbf{d}\right)\left(\mathbf{F}_i^n + \mathbf{G}_i^n\right) + \frac{\Delta t^2}{2}\left(\mathbf{a}_i + \mathbf{b}_i\right)\mathbf{B}^n\right] - \frac{\partial^2}{\partial x_i \partial x_j}\left[\frac{\Delta t^2}{2}\left(\mathbf{a}_i + \mathbf{b}_i\right)\left(\mathbf{F}_j^n + \mathbf{G}_j^n\right)\right] - \left(\Delta t s_5 + \frac{\Delta t^2}{2}\mathbf{d} s_6\right)\mathbf{d}\Delta \mathbf{U}^n - \left(\Delta t + \frac{\Delta t^2}{2}\mathbf{d}\right)\mathbf{B}^n \tag{19}$$

Note that the Beam-Warming Scheme [1] can be written in the form identical to (18) with the following definitions of $\mathbf{E}_i$, $\mathbf{E}_{ij}$ and $\mathbf{Q}^n$

$$\mathbf{E}_i = m\Delta t\left(\mathbf{a}_i + \mathbf{b}_i\right), \qquad \text{with } m = \theta/(1+\xi) \tag{20}$$

$$\mathbf{E}_{ij} = m\Delta t\, \mathbf{c}_{ij} \tag{21}$$

$$\mathbf{Q}^n = \frac{\Delta t}{1+\xi}\left(\frac{\partial \mathbf{F}_i^n}{\partial x_i} + \frac{\partial \mathbf{G}_i^n}{\partial x_i}\right) + \frac{\xi}{1+\xi}\Delta \mathbf{U}^n \tag{22}$$

where the cross derivative terms appearing in $\mathbf{Q}^n$ for the Beam-Warming scheme are included in the second derivative terms on the LHS. The Beam-Warming scheme is seen to be a special case of the FDMEI equations if we set $s_1 = s_3 = m$, $s_2 = s_4 = s_5 = s_6 = 0$, in (18), with adjustments of $\mathbf{Q}^n$ on the RHS. The stability analysis of the Beam-Warming scheme requires $\xi \geq 0.385$ and $\theta = \frac{1}{2} + \xi$. This will fix the implicitness parameter m to be $0.639 \leq m \leq 0.75$. It can be shown that the FDMEI equations as derived in (9) are capable of producing practically all existing FDM and FEM schemes. Some examples are shown in Appendix A.

Contrary to the Beam-Warming scheme, the FDMEI approach is to obtain the implicitness parameters from the current flowfield variables at each and every nodal point rather than by fixing the implicitness parameters to certain predetermined numbers and using them for the entire flow domain irrespective of the local flowfield variation from one point to another. These implicitness parameters may be determined for spatial and temporal bases as depicted in Fig. 2. The final

values of implicitness parameters at any point and at any time can be obtained as the average of both spatial and temporal contributions:

Convection Implicitness Parameters:

$$s_1 = \begin{cases} \min(r,1) & r > \alpha \\ 0 & r < \alpha \ , \ \mathrm{M}_{\min} \neq 0 \\ 1 & \mathrm{M}_{\min} = 0 \end{cases} \qquad s_2 = s_1^n \quad , \quad 0 < n < 1 \tag{23}$$

with

$$r = \sqrt{\mathrm{M}_{\max}^2 - \mathrm{M}_{\min}^2} \,/ \mathrm{M}_{\min} \tag{24}$$

where the maximum and minimum Mach numbers are calculated between adjacent nodal points in FDM or within a local finite element in FEM for spatial implicitness parameters (Fig. 2a) and between the time step at n and $n-1$ for temporal implicitness parameters (Fig. 2b), and α is a user-specified small number ($\alpha \equiv 0.01$). Here it is seen that s_1 is directly related to the flowfield, whereas s_2 depends on s_1 such that $s_2 = s_1^n$. The primary role of s_1 is to ensure the solution accuracy by properly accommodating the convection gradients, whereas that of s_2 is to act as artificial viscosity, for solution stability.

Diffusion Implicitness Parameters:

$$s_3 = \begin{cases} \min(s,1) & s > \beta \\ 0 & s < \beta \ , \ \mathrm{Re}_{\min} \neq 0 \ , \ \text{or } \mathrm{Pe}_{\min} \neq 0 \\ 1 & \mathrm{Re}_{\min} = 0 \ , \ \text{or } \mathrm{Pe}_{\min} = 0 \end{cases} \qquad s_4 = s_3^n \quad , \quad 0 < n < 1 \tag{25}$$

with

$$s = \sqrt{\mathrm{Re}_{\max}^2 - \mathrm{Re}_{\min}^2} \,/ \mathrm{Re}_{\min} \quad \text{or} \quad s = \sqrt{\mathrm{Pe}_{\max}^2 - \mathrm{Pe}_{\min}^2} \,/ \mathrm{Pe}_{\min} \tag{26a,b}$$

where the maximum and minimum Reynolds numbers or maximum and minimum Peclet numbers are calculated similarly as in s_1 for spatial and temporal implicitness parameters, and β is a user-specified small number ($\beta \equiv 0.01$). If temperature gradients are large, it is possible that Peclet numbers instead of Reynolds numbers will dictate the diffusion implicitness parameters. The larger value of s_3 is to be chosen, as obtained either from (26a) or (26b). Note also that $s_4 = s_3^n$ with s_3 ensuring the solution accuracy by taking into account the diffusion gradients, and here again, s_4 plays the role of artificial viscosity, for solution stability.

Source Term Implicitness Parameters:

For the case of chemically reacting flows theDa (Damköhler number) must be used

$$s_5 = \begin{cases} \min(t,1) & t \geq \gamma \\ 0 & t < \gamma \,,\ \mathrm{Da}_{\min} \neq 0 \\ 1 & \mathrm{Da}_{\min} = 0 \end{cases} \qquad s_6 = s_5^n \quad , \quad 0 < n < 1 \tag{27}$$

with

$$t = \sqrt{\mathrm{Da}_{\max}^2 - \mathrm{Da}_{\min}^2} \Big/ \mathrm{Da}_{\min} \tag{28}$$

where the maximum and minimum Damköhler numbers are calculated similarly as in s_1 and s_3 for spatial and temporal implicitness parameters, and γ is a user-specified small number ($\gamma \equiv 0.01$). The relationship between s_5 and s_6 is similar to those for convection and diffusion implicitness parameters such that $s_6 = s_5^n$ with s_5 and s_6 controlling the solution accuracy and solution stability, respectively. The average of both spatial and temporal implicitness parameters will be adopted for use in computations at any point (element) and time.

Relationships between all physical phenomena and the corresponding numerical treatments are characterized by the balance between the first order implicitness parameters (s_1, s_3, s_5) and the second order implicitness parameters (s_2, s_4, s_6), ensuring the computational accuracy and computational stability, respectively. The idea is to provide adequate (no more and no less than required) amount of numerical viscosity in order to preserve the computational accuracy. Note that the definitions for the second order implicitness parameters have been modified from those reported in [15, 16] in order to meet the above requirements (Fig. 3). Initially, it was thought that the second order implicitness parameters should be the direct opposite compliances of the first order implicitness parameters ($s_2 = 1 - s_1$, $s_4 = 1 - s_3$, $s_6 = 1 - s_5$) [16] such that the second order implicitness parameters are the maximum and minimum, respectively, for the minimum and maximum values of the first order implicitness parameters. Unfortunately, such definition resulted in too little numerical viscosities for the high values of the first order implicitness parameters. Subsequently, the limiting values (0.5) of the second order implicitness parameters were provided such that $s_2 = \max(1 - s_1, 0.5)$, etc. as experimented in [15]. However, it was noted that both first and second order parameters should assume the same values at the both extremes at zero and unity with the second order implicitness parameters being reasonably large for all values of the first order implicitness parameters. Thus, the second order implicitness parameters given above are the nonlinear continuous functions of the first order implicitness parameters satisfying these requirements. The range of the constant n is $0 < n < 1$, although $n \equiv \frac{1}{4}$ has been found to be the optimum, exhibiting the best convergence rate for reasonably high CFL numbers in the example problems presented in Section 4.

The flowfield dependent implicitness parameters as defined above are capable of allowing various numerical schemes to be automatically generated, as summarized below:

(1) The first order implicitness parameters s_1 and s_3 control all high gradient phenomena such as shock waves and turbulence. These parameters as calculated from the changes of local Mach numbers and Reynolds (or Peclet) numbers within each element and are indicative of the actual local element flowfields. The contours of these parameters closely resemble

the flowfields themselves, with both s_1 and s_3 being large (close to unity) in regions of high gradients, but small (close to zero) in regions where the gradients are small. The basic role of s_1 and s_3 is to provide computational accuracy.

(2) The second order implicitness parameters s_2 and s_4 are also flowfield dependent. However, their primary role is to provide adequate computational stability (artificial viscosity) as they were originally introduced into the second order time derivative term of the Taylor series expansion of the conservation flow variables $\mathbf{U}^{n+1}$. The primary role of s_2 and s_4 is to provide computational stability.

(3) The s_1 terms represent convection. This implies that if $s_1 \equiv 0$ then the effect of convection is small. The computational scheme is automatically altered to take this effect into account, with the governing equations being predominantly parabolic-elliptic. Note that these effects are confined at $\mathbf{U}^{n+1}$, not at $\mathbf{U}^n$.

(4) The s_3 terms are associated with diffusion. Thus, with $s_3 \equiv 0$, the effect of viscosity or diffusion is small and the computational scheme is automatically switched to that of Euler equations where the governing equations are predominantly hyperbolic.

(5) If the first order implicitness parameters s_1 and s_3 are nonzero, this indicates a typical situation for the mixed hyperbolic, parabolic and elliptic nature of the Navier-Stokes system of equations, with convection and diffusion being equally important. This is the case for incompressible flows at low speeds. The unique property of the FDMEI scheme is its capability to control pressure oscillations adequately without resorting to the separate hyperbolic elliptic pressure equation for pressure corrections. The capability of FDMEI scheme to handle incompressible flows is achieved by a delicate balance between s_1 and s_3 as determined by the local Mach numbers and Reynolds (or Peclet) numbers. If the flow is completely incompressible (M = 0), the criteria given by (19) leads to $s_1 = 1$, whereas the implicitness parameter s_3 is to be determined according to the criteria given in (21). Make a note of the presence of the convection-diffusion interaction terms given by the product of $\mathbf{b}_i\mathbf{a}_j$ in the s_2 terms and $\mathbf{a}_i\mathbf{b}_j$ in the s_4 terms. These terms allow interactions between convection and diffusion in the viscous incompressible and/or viscous compressible flows.

(6) If temperature gradients rather than velocity gradients dominate the flowfield, then s_3 is governed by the Peclet number rather than by the Reynolds number. Such cases arise in high speed, high temperature compressible flows close to the wall.

(7) In the case of reacting flows the source terms $\mathbf{B}$ contains the reaction rates which are functions of the flowfield variables. With widely disparate time and length scales involved in the fast and slow chemical reaction rates of various chemical species as characterized by Damköhler numbers, the first order source term implicitness parameter s_5 is instrumental in dealing with the stiffness of the resulting equations to obtain convergence to accurate solutions. On the other hand, the second order source term implicitness parameter s_6 contribute to the stability of solutions. It is seen that the criteria given by (27-28) will adjust the reaction rate terms in accordance with the ratio of the diffusion time to the

reaction time in finite rate chemistry so as to assure the accurate solutions with computational stability.

(8) Various definitions of Peclet number and Damköhler numbers (Table 1) between the energy and species equations should be checked. Whichever definition provides larger values of s_3 and s_5 must be used. The summary of the above definitions for implicitness parameters is shown in Table 2.

(9) The transition to turbulence is a natural flow process as the Reynolds number increases, causing the gradients of any or all flow variables to increase. This phenomenon is the physical instability and is detected by the increase of s_3 if the flow is incompressible, but by both s_3 and s_1 if the flow is compressible. Such physical instability is likely to trigger the numerical instability, but will be countered by the second order implicitness parameters s_2 and/or s_4 to ensure numerical stability automatically. In this process, these flowfield dependent implicitness parameters are capable of capturing relaminarization, compressibility effect or dilatational turbulent energy dissipation, and turbulent unsteady fluctuations.

(10) An important contribution of the first order implicitness parameters is the fact that they can be used as error indicators for adaptive mesh generations. That is, the larger the implicitness parameters the higher the gradients of any flow variables. Whichever governs (largest first order implicitness parameters) will indicate the need for mesh refinements. In this case, all variables (density, velocity, pressure, temperature, species mass fraction) participate in resolving the adaptive mesh, contrary to the conventional definitions of the error indicators [10,15,16].

(11) Physically, the implicitness parameters will influence the magnitudes of Jacobians. Thus, Item(8) above may be modified so that the diffusion implicitness parameters s_3 and s_4 as calculated from the Reynolds number and Peclet number can be applied to the Jacobians ($\mathbf{a}_i$, $\mathbf{b}_i$, $\mathbf{c}_{ij}$), corresponding to the momentum equations and energy equation, respectively. Furthermore, two different definitions of Peclet number (Pe_I, Pe_{II}) would require the s_3 and s_4 as calculated from the energy and species equations to be applied to the corresponding terms of the Jacobians. Similar applications of the source term implicitness parameters s_5 and s_6 should be followed for the source term Jacobian $\mathbf{d}$ with five different definitions of Damköhler number applied to the corresponding terms of $\mathbf{d}$. In this way, high temperature gradients arising form the momentum and energy equations and the finite rate chemistry governed by the energy and species equations can be resolved accordingly.

The FDMEI equations as given in (13) or (18) may be solved by either FDM or FEM. The standard linear Galerkin approximations of FEM lead to the results of central differences of FDM. However, the main difference between FDM and FEM arises when integration by parts is performed in FEM and the explicit terms of Neumann boundary conditions "naturally" appear as boundary integral forms. Thus, all Neumann boundary conditions can be directly specified at boundaries in FEM. This is not the case for FDM. Often, a rather cumbersome process must be taken for Neumann boundary conditions in FDM.

When dealing with all speed flow regimes such as in shock wave turbulent boundary layer interactions where compressible and incompressible flows, viscous and inviscid flows, and laminar and turbulent flows are intermingled throughout the flowfield domain, a computational scheme intended for only one type of flow physics and that does not account for other types of flow phenomena will fail. For example, the flow close to the wall in shock wave turbulent boundary layer interactions is incompressible ($M \leq 0.1$), whereas away from the wall the flow is compressible (supersonic or hypersonic). In this case, viscous flows change to inviscid flows. In between these two extremes the flowfield changes continuously, oscillating back and forth across the boundary layers of velocity and entropy, and leading edge and bow shocks. At any given computational nodal point or element, gradients of each variable (density, pressure, velocity, and temperature) may be very small or very large, so large that practically all currently available computational methods may fail. In order to succeed, it is necessary that the current flow physics everywhere be identified and so recognized, with specific computational schemes accorded to each and every computational nodal point and element. It is clear that such accommodations are available in (13) or (18).

3. IMPLEMENTATION AND COMPUTATIONAL PROCESS

As stated earlier, the governing equations for the Taylor series-modified Navier-Stokes system of equations, (13) or (18) may be applied to either FDM or FEM, or to the finite volume method (FVM). For application to FDM any of the existing finite difference methods can be used to obtain the standard finite difference analogs for either (13) or (18) such as the central schemes, upwinding schemes, or TVD schemes. The role of the FDMEI is them to enhance the computational accuracy above and beyond the limit of the current FDM capabilities.

For applications to FEM we begin by expressing the conservation and flux variables and source terms as a linear combination of trial functions Φ_α with the nodal values of these variables.

$$\begin{aligned} \mathbf{U}(\mathbf{x},t) &= \Phi_\alpha(\mathbf{x})\,\mathbf{U}_\alpha(t) \quad , \quad & \mathbf{F}_i(\mathbf{x},t) &= \Phi_\alpha(\mathbf{x})\,\mathbf{F}_{\alpha i}(t) \\ \mathbf{G}_i(\mathbf{x},t) &= \Phi_\alpha(\mathbf{x})\,\mathbf{G}_{\alpha i}(t) \quad , \quad & \mathbf{B}(\mathbf{x},t) &= \Phi_\alpha(\mathbf{x})\,\mathbf{B}_\alpha(t) \end{aligned} \tag{29}$$

Applying the generalized Galerkin approximations to (11) we obtain

$$\int_\Omega \Phi_\alpha \mathbf{R}(\mathbf{U},\mathbf{F}_i,\mathbf{G}_i,\mathbf{B})\,d\Omega = 0 \tag{30}$$

or

$$\left(A_{\alpha\beta}\eta_{rs} + B_{\alpha\beta rs}\right)\Delta U^{n+1}_{\beta s} = H^n_{\alpha r} + N^n_{\alpha r} \tag{31}$$

where

$$A_{\alpha\beta} = \int_\Omega \Phi_\alpha \Phi_\beta \, d\Omega \tag{32}$$

$$\eta_{rs} = \delta_{rs} - s_5 \Delta t d_{rs} - s_6 \tfrac{1}{2}\Delta t^2 d_{rt} d_{ts} \tag{33}$$

$$B_{\alpha\beta rs} = \int_{\Omega}\Bigg[-\Big\{\Delta t\left(s_1 a_{irs} + s_3 b_{irs}\right) + \frac{\Delta t^2}{2}\left[s_2 d_{rt} a_{its} + s_6 d_{rt}\left(a_{its} + b_{its}\right) + s_4 d_{rt} b_{its}\right]\Big\}\Phi_{\alpha,i}\Phi_{\beta}$$
$$-\Big\{\Delta t\, s_3 c_{ijrs} - \frac{\Delta t^2}{2}\left[s_2\left(a_{irt}a_{jts} + b_{irt}a_{jts}\right) + s_4\left(a_{irt}b_{jts} + b_{irt}b_{jts} - d_{rt}c_{ijts}\right)\right]\Big\}\Phi_{\alpha,i}\Phi_{\beta,j}\Bigg] d\Omega$$
$$+\int_{\Gamma}\Bigg[\Big\{\Delta t\left(s_1 a_{irs} + s_3 b_{irs}\right) + \frac{\Delta t^2}{2}\left[s_2 d_{rt} a_{its} + s_6 d_{rt}\left(a_{its} + b_{its}\right) + s_4 d_{rt} b_{its}\right]\Big\}\dot{\Phi}_{\alpha}\dot{\Phi}_{\beta}$$
$$+\Big\{\Delta t\, s_3 c_{ijrs} - \frac{\Delta t^2}{2}\left[s_2\left(a_{irt}a_{jts} + b_{irt}a_{jts}\right) + s_4\left(a_{irt}b_{jts} + b_{irt}b_{jts} - d_{rt}c_{ijts}\right)\right]\Big\}\dot{\Phi}_{\alpha}\dot{\Phi}_{\beta,j}\Bigg] n_i\, d\Gamma \tag{34}$$

$$H^n_{\alpha r} = \int_{\Omega}\Bigg\{\Bigg[\Delta t\left(F^n_{\beta ir} + G^n_{\beta ir}\right) + \frac{\Delta t^2}{2} d_{rs}\left(F^n_{\beta is} + G^n_{\beta is}\right) + \frac{\Delta t^2}{2}\left(a_{irs} + b_{irs}\right)B^n_{\beta s}\Bigg]\Phi_{\alpha,i}\Phi_{\beta}$$
$$-\frac{\Delta t^2}{2}\left(a_{irs} + b_{irs}\right)\left(F^n_{\beta js} + G^n_{\beta js}\right)\Phi_{\alpha,i}\Phi_{\beta,j} + \left(\Delta t B^n_{\beta r} + \frac{\Delta t^2}{2} d_{rs} B^n_{\beta s}\right)\Phi_{\alpha}\Phi_{\beta}\Bigg\} d\Omega \tag{35}$$

$$N^n_{\alpha r} = \int_{\Gamma}\Bigg\{\Bigg[-\Delta t\left(F^n_{\beta ir} + G^n_{\beta ir}\right) - \frac{\Delta t^2}{2} d_{rs}\left(F^n_{\beta is} + G^n_{\beta is}\right) - \frac{\Delta t^2}{2}\left(a_{irs} + b_{irs}\right)B^n_{\beta s}\Bigg]\dot{\Phi}_{\alpha}\dot{\Phi}_{\beta}$$
$$+\frac{\Delta t^2}{2}\left(a_{irs} + b_{irs}\right)\left(F^n_{\beta js} + G^n_{\beta js}\right)\dot{\Phi}_{\alpha}\dot{\Phi}_{\beta,j}\Bigg\} n_i\, d\Gamma \tag{36}$$

where all Jacobians must be updated at each time step and $\dot{\Phi}_{\alpha}$ represents the Neumann boundary trial and test functions, with α, β denoting the global node number and r, s providing the number of conservation variables at each node. For three dimensions, $i, j = 1, 2, 3$ associated with the Jacobians imply directional identification of each Jacobian matrix ($\mathbf{a}_1$, $\mathbf{a}_2$, $\mathbf{a}_3$, $\mathbf{b}_1$, $\mathbf{b}_2$, $\mathbf{b}_3$, $\mathbf{c}_{11}$, $\mathbf{c}_{12}$, $\mathbf{c}_{13}$, $\mathbf{c}_{21}$, $\mathbf{c}_{22}$, $\mathbf{c}_{23}$, $\mathbf{c}_{31}$, $\mathbf{c}_{32}$, $\mathbf{c}_{33}$) with $r, s = 1, 2, 3, 4, 5$ denoting entries of each of the 5×5 Jacobian matrices.

It is important to realize that the integration by parts as applied to the generalized Galerkin approximations in FEM produces all Neumann boundary integrals. It is particularly advantageous that Neumann boundary conditions through re-evaluation of Jacobians normal to the boundary surfaces can simply be added to the boundary nodes for the stiffness matrix $B_{\alpha\beta rs}$ in (34). On the other hand, all Neumann boundary conditions which appear in (36) act as source terms. These features are absent in FDM, but implementations of Neumann boundary conditions can be handled by devising special forms of finite differences at boundary nodes.

The generalized Galerkin approach of (13) may be replaced by the generalized Petrov-Galerkin methods. This process will require the RHS of (34) and (35) to be revised by adding, respectively,

$$\int_{\Omega} E_{irs}\beta g_j \Phi_{\alpha,i}\Phi_{\beta,j}d\Omega$$

$$-\int_{\Omega} \overline{E}_{irs}\beta g_j \Phi_{\alpha,i}\Phi_{\beta,j}d\Omega$$

with E_{irs} being the quantities inside of the brackets of the convection terms in (34) and $\overline{E}_{irs}$ are those in (34) and βg_i are the Petrov-Galerkin parameters as defined in (A20), Appendix A. The role of the FDMEI is, as in FDM of different schemes, to enhance the solution accuracy above and beyond the Petrov-Galerkin methods. Otherwise, the formulation given by (13) represents the generalized Taylor-Galerkin method with accuracy enhanced by the FDMEI scheme.

Similar results are obtained either by FDM or FEM with accuracy of computations derived primarily from the FDMEI equations of (13) or (18). However, with the increase of Reynolds number (say around Re $>>10^8$), it is possible that accuracy may increase with applications of special functions such as Legendre polynomials of high degree modes characterizing extremely small turbulent microscales. Implementation of such high frequency modes can be achieved by placing these modes between the corner nodes of isoparametric finite elements. Adaptively, such high modes can be chosen as needed for the resolution of turbulent microscales. Once again the diffusion implicitness parameter s_3 will play a crucial factor in determining the required degrees of Legendre polynomial. The use of Legendre polynomial spectral modes superimposed onto isoparametric elements has been discussed in [9,12,15]. Its merit, however, has not yet been fully established for general applications.

For turbulent flows with an extremely high Reynolds number, the phase error of the short wavelengths can be very large. In this case, it is necessary to add numerical dissipation terms to damp out the short wavelengths. Such numerical viscosities are conceptually different from the second order implicitness parameters whose role is to ensure stable solutions while preserving the solution accuracy dictated by the first order implicitness parameters. Toward this end, it is desirable to revise (18) in the form

$$\left(\mathbf{I}+\frac{\partial \mathbf{E}_i}{\partial x_i}+\frac{\partial^2 \mathbf{E}_{ij}}{\partial x_i \partial x_j}\right)\Delta \mathbf{U}^{n+1} = -\mathbf{Q}^n - \overline{\mathbf{Q}}^n \tag{37}$$

where $\overline{\mathbf{Q}}^n$ is the numerical dissipation vector in terms of the second order tensor of numerical dissipation, S_{ij}, associated with the second order derivatives of $\mathbf{U}^n$,

$$\overline{\mathbf{Q}}^n = S_{ij}\frac{\partial^2 \mathbf{U}^n}{\partial x_i \partial x_j} = \overline{\mu}\Delta x_i \Delta x_j \frac{\partial^2 \mathbf{U}^n}{\partial x_i \partial x_j} \tag{38}$$

with $\overline{\mu}$ being the numerical dissipation constant chosen as $0 \le \overline{\mu} \le \overline{\mu}_o$, where $\overline{\mu}_o$ is set approximately equal to 2, but adjusted from numerical experiments. Note that the Galerkin integral of (38) (integration by parts once) leads to the first derivative of the trial and test functions combined with the nodal values of $\mathbf{U}^n_\beta$. In addition, note that the damping provided by the second order derivatives will not disrupt the formal accuracy of the FDMEI scheme. This process may be applied to (13) as well.

One of the most significant aspects of the FDMEI scheme is that for low Mach numbers (incompressible flow) the scheme will automatically adjust itself to prevent pressure oscillations. This adjustment is analogous to the pressure correction scheme employed for incompressible flows. Otherwise, the FDMEI scheme is capable of shock wave resolutions at high Mach numbers, and particularly well suited for dealing with interactions between shock waves and turbulent boundary layers where regions of high and low Mach numbers and Reynolds numbers coexist. In this case, the inviscid and viscous interactions are allowed to take place. To this end the second order implicitness parameters play the role of artificial viscosity needed for shock wave resolutions in the presence of flow diffusion due to physical viscosity.

In order to understand how the FDMEI scheme handles computations involving both compressible and incompressible flows fundamental definitions of pressure must be recognized. Consider in the following that the fluid is a perfect gas and that the total energy is given by

$$E = c_p T - \frac{p}{\rho} + \frac{1}{2} v_i v_i \tag{39}$$

The momentum equation for steady state incompressible rotational flow may be integrated to give

$$\int \left(p + \tfrac{1}{2}\rho v_j v_j\right)_{,i} dx_i = \int \left[\mu\left(v_{i,jj} + \tfrac{1}{3} v_{j,ji}\right) + \rho \varepsilon_{ijk} v_j \omega_k\right] dx_i$$

$$p + \tfrac{1}{2}\rho v_j v_j = p_o + W \tag{40}$$

with

$$W = \frac{1}{m}\int \left[\mu\left(v_{i,jj} + \tfrac{1}{3} v_{j,ji}\right) + \rho \varepsilon_{ijk} v_j \omega_k\right] dx_i$$

where ω_k is the component of a vorticity vector, p_o is the constant of integration, and m denotes the spatial dimension.

Combining (39) and (40) leads to the following relationship:

$$p_o = \rho\left(c_p T + v_i v_i - E\right) - W \tag{41}$$

If p_o as given by (41) remains a constant, equivalent to a stagnation pressure, then the compressible flow as assumed in the conservation form of the Navier-Stokes system of equations has now been turned into an incompressible flow, which is expected to occur when the flow velocity is sufficiently reduced (approximately $0.1 \le M < 0.3$ for air). Thus, (41) may serve as an equivalent equation of state for an incompressible flow. This can be identified element by element for the entire domain. Note that conservation of mass is achieved for incompressible flows with p_o in (41) being constant, thus keeping the pressure from oscillating.

Once the Navier-Stokes solution via FDMEI is carried out and all flow variables determined, then we compute fluctuations f' of any variable f,

$$f' = f - \bar{f} \tag{42}$$

where f and $\bar{f}$ denote the Navier-Stokes solution and its time average, respectively. This process may be replaced by the fast Fourier transform of the Navier-Stokes solution. Unsteady turbulence statistics (turbulent kinetic energy, Reynolds stresses, and various energy spectra) can be calculated once the fluctuation quantities of all variables are determined.

Before we demonstrate numerical examples, let us summarize why the FDMEI scheme is capable of handling low speed and high speed and compressible and incompressible flows, including shock waves and turbulent flows: (1) How is the transition from incompressible flow to compressible flow naturally and automatically accommodated without using two separate equations or two separate codes? This process is dictated by the first order convection implicitness parameter s1 as reflected by the Mach number changes and the expression of the stagnation pressure. (2) How is the shock wave captured? As the Mach number increases and its discontinuity is abrupt, the s_2 terms associated with second order derivatives together with squares of the convection Jacobian provide adequate numerical viscosities through second order derivatives, similarly as the Lax-Wendroff scheme. (3) How is the transition from laminar to turbulent flows naturally and automatically accommodated? This process is governed by the first and second order diffusion implicitness parameters (s_3 and s_4) as calculated from the changes of the Reynolds number. The terms associated with s_3 and s_4 are responsible for fluctuations of velocities, with the values of these implicitness parameters increasing with intensities of turbulence in conjunction with the diffusion gradient Jacobian and the squares of the diffusion Jacobian. This process allows the Navier-Stokes solutions to contain fluctuations which can be extracted by subtracting the time averages of the Navier-Stakes solutions. (4) How do the interactions between convection and diffusion take place? Changes of Mach numbers and Reynolds numbers as reflected by both convection and diffusion implicitness parameters close to the wall contribute to the unsteadiness. Away from the wall, they contribute to the transition between incompressible to compressible flows. (5) How are the stiff equations arising from widely disparate reaction rates of all chemical species treated? The most crucial aspect of the FDMEI scheme is its capability to identify the ratio of the resident time to the reaction time as calculated from five different definitions of the Damköhler numbers between the adjacent nodal points and time steps as reflected in the calculated first order implicitness parameter, s_5, and the second order implicitness parameter, s_6. These parameters provide precise degree of computational implicitness at every nodal point and every time step, contributing to the determination of accurate chemical reactions.

4. APPLICATIONS

We examine here various example problems:(a) flow over a flat plate, (b) shock wave turbulent boundary layer interactions on a compression corner, (c) 3D duct flows, and (d) lid-driven cavity flow. Linear isoparametric finite elements are used for the example problems.

(a) *Behavior of Flowfield Dependent Implicitness Parameters on Flat Plate*

First of all, our concern is to test the behavior of FDMEI and FDMEI-FEM. Toward this objective we examine the flow over a flat plate investigated earlier by Carter [17] as shown in Fig. 4a. The initial setting for the implicitness parameters are determined from the initial conditions of

the flowfield and subsequently updated after each time step until the steady state solution is reached.

Corresponding to the mesh refinements and the flowfields at steady state shown in Fig. 4b, c, d, the contours of implicitness parameters s_1 and s_3 are given in Fig. 5. It is seen that the implicitness parameters themselves closely resemble the flowfield. There are little or no changes in Mach numbers and Reynolds numbers between adjacent nodes or elements far away from the surface of the plate as indicated by $s_1 = s_3 = 0$. Along the leading edge shock and boundary layers, both s_1 and s_3 move toward unity indicating that gradients of all variables increase. The final flowfields, as shown in Fig. 4b,c,d, are the consequence of these implicitness parameters. The implicitness parameters s_2 and s_4 are the compliances of s_1 and s_3, respectively, with their primary roles being the artificial viscosity. Thus, the first order implicitness parameters (s_1, s_3) help to resolve the high gradients ensuring the accuracy of the solution. While on the other hand, the second order implicitness parameters (s_2, s_4) ensure computational stability.

Computations of wall pressure, wall skin friction, u-velocity, v-velocity, density and temperature distribution are shown in Figs. 6a through 6f. The comparison with the Carter's data indicates reasonable agreements.

(b) ***Supersonic Flow on a Compression Corner***

In this example we demonstrate calculations of supersonic flow on a compression corner. The inlet boundary conditions (non-dimensionalized) are $\rho = 1$, $M = 2.25$, $p = 0.14$, $Re = 105$, $Pr = 0.72$, and $v = 0$, with adiabatic wall condition. The steady state background mean flowfields for the compression corner are shown in Fig 7a. In these calculations, all perturbation (fluctuation) variables are determined from time averages of the Navier-Stokes solutions according to (35). The horizontal and vertical perturbation velocities (u', v') at locations close to the wall ($x = 0.10256$ m, $y = 0.001$ m) and away from the wall ($x = 0.10256$ m, $y = 0.04$ m) are shown in Fig. 7b. Note that u' is extremely unsteady whereas v' is significantly less unsteady close to the wall. Away from the wall, both u' and v' are almost steady. These trends are reflected in the turbulence (Reynolds) stresses as shown in Fig 7c. Turbulent kinetic energy distributions at the locations upstream of the corner ($x = 0.0513$ m) and downstream of the corner ($x = 0.1333$ m) are shown in Fig 7d. We observe that the turbulent kinetic energy downstream of the corner is significantly larger than the upstream. No turbulent statistics calculations (wave numbers or frequencies vs power spectral density) are attempted at this time as turbulence microscales are not resolved in this example.

It should be noted that the above results obtained without turbulence models or without the standard DNS solutions (neither spectral nor DNS-mesh refinements) are regarded as the consequence of the time-averaging of the FDMEI Navier-Stokes solutions. This implies that the fluctuation of variables between nodal points (Fig 2a) and between time steps (Fig 2b) as reflected in terms of the implicitness parameters (s_i) have contributed to these physical phenomena, with compressibility and shock waves dictated by the Mach number-dependent s_1, and with incompressibility and turbulent fluctuations dictate by the Reynolds number or Peclet number-dependent (s_3). An equal participation of s_1 and s_3 will be responsible for shock wave turbulent boundary layer interactions. A comparison of the results of the FDMEI scheme with the κ-ε

turbulent model and experimental data is shown in Fig 7e. It is seen that the FDMEI results compare more favorably with those of measurements [18].

(c) ***FDMEI Analysis of Three Dimensional Flows***

To demonstrate the effectiveness of the flowfield-dependent implicitness parameters in 3-D flows at the steady state, we examine the spatially evolving boundary layer (Figs. 8a through 8e). Note that the contours of s_1 and s_3 (Fig. 8c) show the boundary layer effects in which both s_1 and s_3 are indicative of rapid changes of Mach numbers and Reynolds numbers respectively, larger (close to unity) on the wall, but small (closer to zero) away from the wall. The velocity vectors and RMS error distributions versus interactions are shown in Figs. 8d and 8e, respectively.

(d) ***Demonstration of Compressibility vs Incompressibility***

We ask the question: Can a single formulation or computer program originally designed for high speed compressible flows be applied to analyze the low speed incompressible flows? The advantage of FDMEI is to respond positively to this question. To prove the point, let us examine the lid-driven cavity flow at the steady state (Figs. 9a through 9f). Notice that, for M = 0.1, density changes occur closer to the lid, whereas, for M = 0.01, density is constant throughout the domain (Fig. 9e), corresponding to P_o being variable and constant, respectively (see Eq. (32)). The equation of state for compressible flows is automatically switched over to accommodate the incompressible flows. This advantage is contrary to the previous practice such as the Table look-up for the equation of state for incompressible flow handled separately through hyperbolic elliptic equation as derived from the continuity equation combined with the momentum and energy equations. Comparisons of the results of FDMEI with those of the independent incompressible flow code of Ghia et al [19] are very favorable as shown in Figs. 9a through 9f.

5. CONCLUDING REMARKS

The validity of the proposed new approach to computational fluid dynamics has been demonstrated through some example problems. Excluded from these examples are reacting flows which are reported elsewhere [16]. Also excluded is the effect of additional spectral modes of Legendre polynomials which are described in [15]. None of the example problems have been carried out with mesh refinements required for resolving turbulent microscales due to the limitation of computer time. The following concluding remarks are provided:

(a) The flowfield-dependent implicitness parameters as calculated from the current flowfield information are indicative of the magnitude of gradients of all variables and adjust the computational schemes accordingly for every nodal point or element, rather than dictated by arbitrarily selected constant parameters throughout the domain.

(b) The first order implicitness parameters s_1, s_3, and s_5 as calculated from Mach numbers, Reynolds or Peclet numbers, and Damköhler numbers, respectively, ensure the solution accuracy, whereas the second order implicitness parameters s_2, s_4, and s_6 which are determined as compliances of s_1, s_3, and s_5. respectively, assist in the solution stability.

(c) The FDMEI method is capable of resolving mutual interactions and transition between

viscous and inviscid flows, compressible and incompressible flows, and laminar and turbulent flows, in all speed regimes.

(d) Further research on FDMEI is required in order to investigate many other physical phenomena including hypersonics and reacting flows with high temperatures in 3D geometries.

REFERENCES

1. Beam. R. M. and Warming, R. F. [1978]: 'An Implicit Finite-Difference Algorithm for Hyperbolic Systems in Conservation Law Form,' *Journal of Computational Physics, Vol.* 22, pp. 87-110.
2. Harten, A. [1983]: 'High resolution schemes for hyperbolic conservation laws.' *Journal Computational Physics, 49,* 357-93.
3. MacCormack. R. W. [1988]: 'Current Status of Numerical Solutions of the Navier-Stokes Equations,' AIAA paper 88-0513.
4. Briley, W. R. and McDonald, H. [1980]: On the Structure and Use of Linearized Block Implicit Schemes, *J. Comp. Phys.*, Vol. 34, pp. 54-73.
5. Jameson, A., Schmidt, W. and Turkel, E. [1981]: 'Numerical simulation of the Euler equations by finite volume methods using Runge-Kutta time stepping schemes.' *AIAA Paper 81-1259, AIAA* 5th Computational Fluid Dynamics Conference.
6. Hirsch, C. [1988]: *Numerical Computation of Internal and External Flows,* Vol. I: *Fundamentals of Numerical Discretization,* Wiley, New York.
7. Hirsch, C. [1990]: *Numerical Computation of Internal and External Flows,* Vol. II: *Computational Methods for Inviscid and Viscous Flows,* Wiley, New York.
8. Chung, T. J. [1978]: *Finite Element Analysis in Fluid Dynamics,* McGraw-Hill, New York.
9. Babuska. I and Suri, M. [1987]: 'The *h-p* Version of the Finite Element Method with Quasi-Uniform Meshes.' *Math. Model. Numer. Anal.* (RAIRO), 21, pp. 199-235.
10. Oden, J., Demkowicz, L., Rachowicz, W. and Westermann [1989]: 'Toward a Universal h-p Adaptive Finite Element Strategy: Part II. A Posteriori Error Estimation', *Computer Methods in Applied Mechanics and Engineering,* Vol. 77, pp. 113-180.
11. Hughes, T.J.R., Franca, L., and Mallet, M., [1986]: A New Finite Element Formulation for Computational Fluid Dynamics: I. Symmetric Forms of the Compressible Euler and Navier—Stokes Equations and the Second Law of Thermodynamics, *Comp. Meth. Appl. Mech. Eng. 54,* pp. 223—234.
12. Oden, J.T. [1993]: 'Theory and Implementation of High-Order Adaptive hp-methods for the Analysis of Incompressible Viscous Flows,' *Computations in Nonlinear Mechanics in Aerospace Engineering, AIAA Progress in S.N. Atluri (ed)* .
13. Hassan, O., Morgan, K. and Peraire, J. [1991]: 'An Implicit Explicit Element Method for High-Speed Flows', *Int J for Num Meth in Engrg,* Vol. 32 (1), July 1991, p. 183.
14. Zienkiewicz. O., Codina. R. [1995]: A General Algorithm for Compressible and Incompressible Flow-Part I. The Split, Characteristic-Based Scheme", Int. J. Numer. Meth. in Fluids, Vol. 20, pp. 869-885.
15. Yoon, K.T. and Chung, T.J. [1996]: 'Three-Dimensional Mixed Explicit-Implicit Galerkin Spectral Element Methods for high Speed Turbulent Compressible Flows,' *Computer Methods in Applied Mechanics and Engineering,* Vol. 135, pp.343-367.
16. Moon, S.Y, K. T. Yoon, and Chung, T.J. [1996]: 'Numerical Simulation of Heat Transfer in Chemically Reacting Shock Wave Turbulent Boundary Layer Interactions,' *Numerical Heat Transfer,* Vol. 30, Part A, pp. 55-72.
17. Carter, J. E. [1972]: Numerical Solutions of the Navier Equations for the Supersonic Laminar Flow Over a Two- dimensional Compression Corner,' NASA TR-R-385.
18. Ardonceau. P. Lee, D.H., Alziary de Roguefort, T., and Goethals, R., [1980]: 'Turbulence Behavior in a Shock Wave/Boundary Layer Interactions,' AGARD CP-271, paper No. 8
19. Ghia, U., Ghia, K., and Shin, C.T. [1982]:. 'High Resolution for Incompressible flow using the Navier Stokes Equations and a Multigrid Method.' *Journal of Computational Physics,* Vol. 48, pp. 387-411.

Table 1 Definitions of Nondimensional Flowfield Quantities

$$\underbrace{\rho(\mathbf{v}\cdot\nabla)\mathbf{v}}_{\mathrm{A}} = \underbrace{-\nabla p}_{\mathrm{B}} + \underbrace{\mu\left[\nabla^2\mathbf{v} + \tfrac{1}{3}\nabla(\nabla\cdot\mathbf{v})\right]}_{\mathrm{C}}$$

$$\underbrace{\nabla\cdot\rho\mathbf{v}\int_{T_o}^{T} c_{pk}\,dT}_{\mathrm{E}} - \underbrace{\nabla\cdot k\nabla T}_{\mathrm{F}} - \underbrace{\nabla\cdot\left(\rho D\nabla Y_k\int_{T_o}^{T} c_{pk}\,dT\right)}_{\mathrm{G}} = \underbrace{-\sum_{k=1}^{N} H_k^o w_k}_{\mathrm{N}}$$

$$\underbrace{\nabla\cdot(\rho Y_k\,\mathbf{v})}_{\mathrm{I}} - \underbrace{\nabla\cdot(\rho D\nabla Y_k)}_{\mathrm{J}} = \underbrace{w_k}_{\mathrm{K}}$$

Mach number	M	$\frac{u}{a}$	$\frac{\mathrm{A}}{\mathrm{B}} = \frac{\text{inertial force}}{\text{pressure force}}$
Reynolds number	Re	$\frac{\rho u L}{\mu}$	$\frac{\mathrm{A}}{\mathrm{C}} = \frac{\text{inertial force}}{\text{viscous force}}$
Peclet number, I	Pe_{I}	$\frac{\rho u L c_{pk}}{k}$	$\frac{\mathrm{E}}{\mathrm{F}} = \frac{\text{convective heat transfer}}{\text{conductive heat transfer}}$
Peclet number, II	$\mathrm{Pe}_{\mathrm{II}}$	$\frac{uL}{D}$	$\frac{\mathrm{I}}{\mathrm{J}} = \frac{\text{convective mass transfer}}{\text{diffusive mass transfer}}$
Damköhler number, I	Da_{I}	$\frac{L w_k}{\rho u Y_k}$	$\frac{\mathrm{K}}{\mathrm{I}} = \frac{\text{mass source}}{\text{convective mass transfer}}$
Damköhler number, II	$\mathrm{Da}_{\mathrm{II}}$	$\frac{L^2 w_k}{\rho D Y_k}$	$\frac{\mathrm{K}}{\mathrm{J}} = \frac{\text{mass source}}{\text{diffusive mass transfer}}$
Damköhler number, III	$\mathrm{Da}_{\mathrm{III}}$	$\frac{qL}{Hu}$	$\frac{\mathrm{N}}{\mathrm{E}} = \frac{\text{heat source}}{\text{convective heat transfer}}$
Damköhler number, IV	$\mathrm{Da}_{\mathrm{IV}}$	$\frac{qL^2}{kT}$	$\frac{\mathrm{N}}{\mathrm{F}} = \frac{\text{heat source}}{\text{conductive heat transfer}}$
Damköhler number, V	Da_{V}	$\frac{qL^2}{HD}$	$\frac{\mathrm{N}}{\mathrm{G}} = \frac{\text{heat source}}{\text{diffusive heat transfer}}$

Table 2 Flowfield Dependent Implicitness Parameters

<table>
<tr><td rowspan="5">Convection gradient behavior</td><td colspan="2">s_1 - First order convection implicitness parameter</td></tr>
<tr><td>$$s_1 = \begin{cases} \min(r,1) & r > \alpha \\ 0 & r < \alpha \ , \ \mathrm{M}_{\min} \neq 0 \\ 1 & \mathrm{M}_{\min} = 0 \end{cases}$$
$$r = \sqrt{\mathrm{M}_{\max}^2 - \mathrm{M}_{\min}^2} \,/\, \mathrm{M}_{\min}$$</td><td>Ensures solution accuracy. Strongly flowfield dependent, with high gradients characterized by large Mach number changes between nodal points or within element and between time steps.</td></tr>
<tr><td colspan="2">s_2 - Second order convection implicitness parameter</td></tr>
<tr><td>$s_2 = s_1^n \quad , \quad 0 < n < 1$</td><td>Ensures solution stability. Flowfield dependent artificial viscosity for convection process</td></tr>
<tr><td rowspan="5">Diffusion gradient behavior</td><td colspan="2">s_3 - First order diffusion implicitness parameter</td></tr>
<tr><td>$$s_3 = \begin{cases} \min(s,1) & s > \beta \\ 0 & s < \beta \ , \ \mathrm{Re}_{\min} \neq 0 \ , \ \text{or } \mathrm{Pe}_{\min} \neq 0 \\ 1 & \mathrm{Re}_{\min} = 0 \ , \ \text{or } \mathrm{Pe}_{\min} = 0 \end{cases}$$
$$s = \sqrt{\mathrm{Re}_{\max}^2 - \mathrm{Re}_{\min}^2} \,/\, \mathrm{Re}_{\min} \quad \text{or} \quad s = \sqrt{\mathrm{Pe}_{\max}^2 - \mathrm{Pe}_{\min}^2} \,/\, \mathrm{Pe}_{\min}$$</td><td>Ensures solution accuracy. Strongly flowfield dependent, with high gradients characterized by large changes in Reynolds number or Peclet number between nodal points or within element and between time steps. Diffusion gradient behavior may be dictated by Peclet number when temperature gradients are high. Choose whichever (Reynolds or Peclet number) provides the larger value for s.</td></tr>
<tr><td colspan="2">s_4 - Second order diffusion implicitness parameter</td></tr>
<tr><td>$s_4 = s_3^n \quad , \quad 0 < n < 1$</td><td>Ensures solution stability. Flowfield dependent artificial viscosity for diffusion process</td></tr>
<tr><td rowspan="5">Source term gradient behavior</td><td colspan="2">s_5 - First order source term implicitness parameter</td></tr>
<tr><td>$$s_5 = \begin{cases} \min(t,1) & t \geq \gamma \\ 0 & t < \gamma \ , \ \mathrm{Da}_{\min} \neq 0 \\ 1 & \mathrm{Da}_{\min} = 0 \end{cases}$$
$$t = \sqrt{\mathrm{Da}_{\max}^2 - \mathrm{Da}_{\min}^2} \,/\, \mathrm{Da}_{\min}$$</td><td>Ensures solution accuracy. Strongly flowfield dependent, with high reaction rate gradients characterized by large Damköhler number changes between nodal points or within element and between time steps.</td></tr>
<tr><td colspan="2">s_6 - Second order source term implicitness parameter</td></tr>
<tr><td>$s_6 = s_5^n \quad , \quad 0 < n < 1$</td><td>Ensures solution stability. Flowfield dependent artificial viscosity for reaction process</td></tr>
</table>

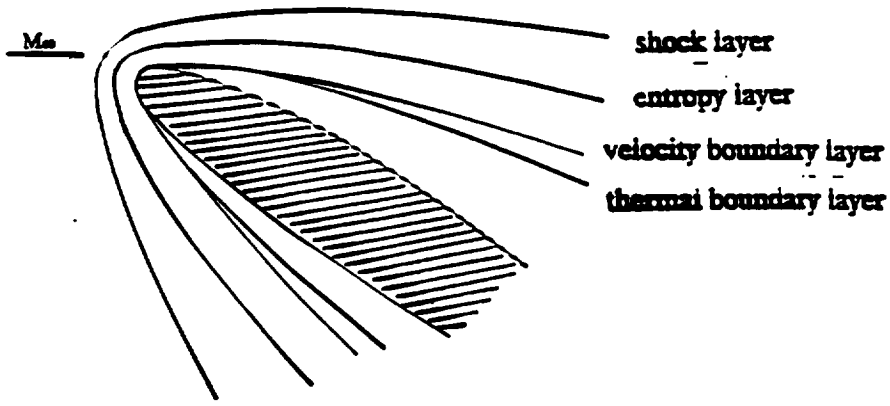

(a) External flow over a blunt body

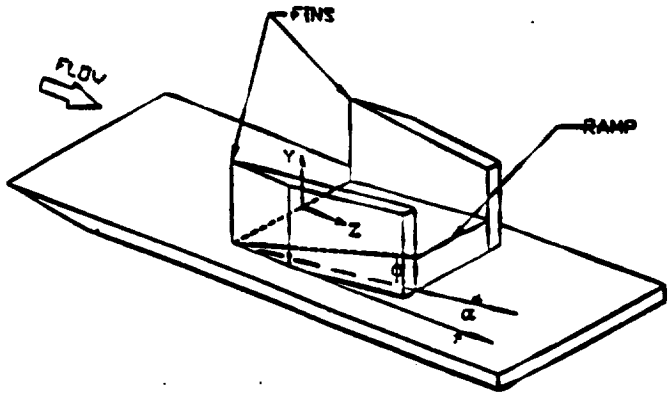

(b) Internal flow through fins

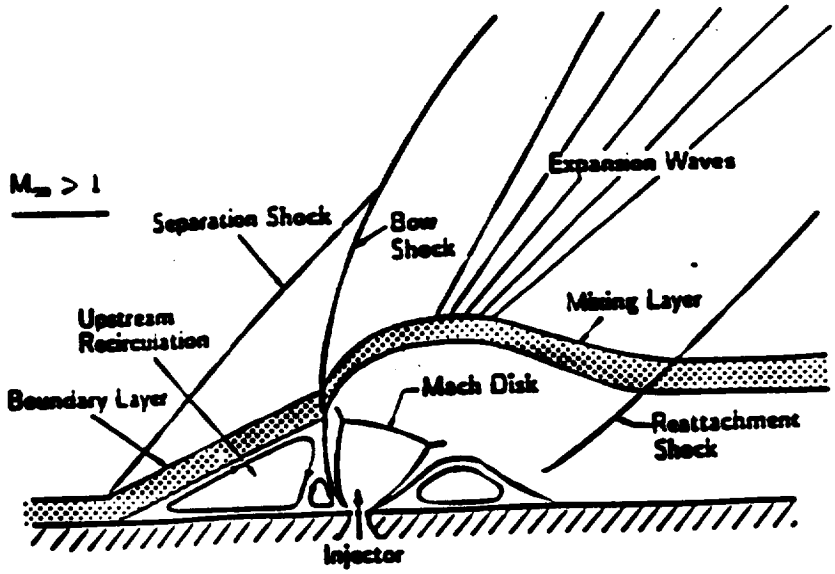

(c) Reacting flow (air-breathing combustion)

Fig 1 Supersonic and Hypersonic Flows

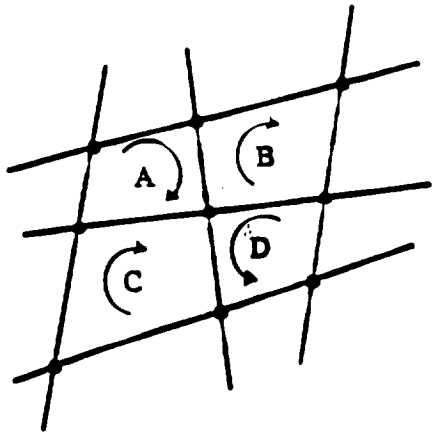

(a) Idealized turbulence length scales assumed to be within each element - spatially evolving turbulence. The maximum and minimum values of M, Re, Pe, and Da are those among the corner nodes within an element.

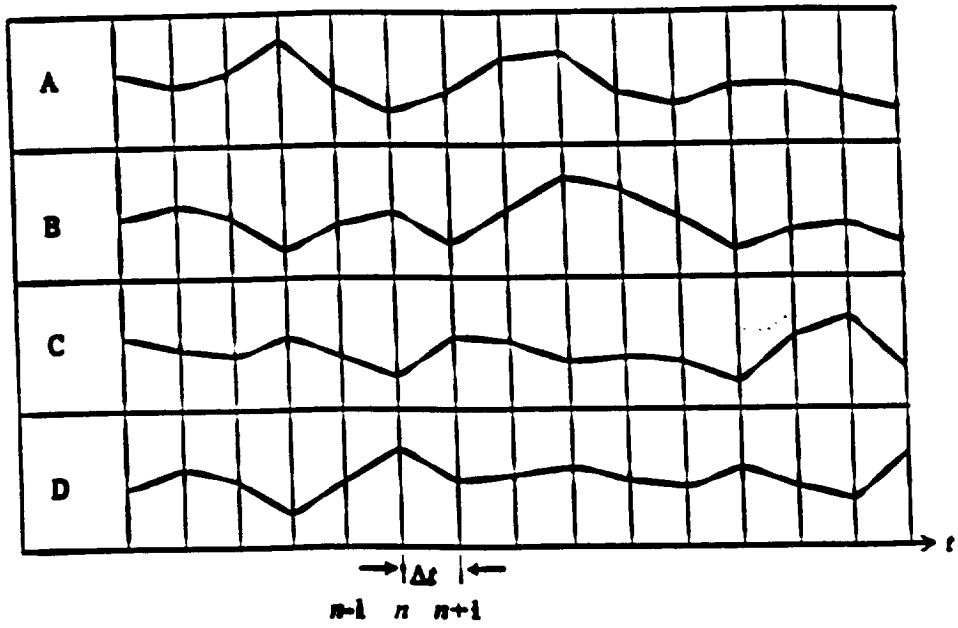

(b) Idealized turbulence time scales assumed to be within each time step - temporally evolving turbulence. The maximum and minimum values of M, Re, Pe, and Da are identified at time steps n and $n-1$.

Fig 2 Spatial and Temporal Flowfield Dependent Implicitness Parameters

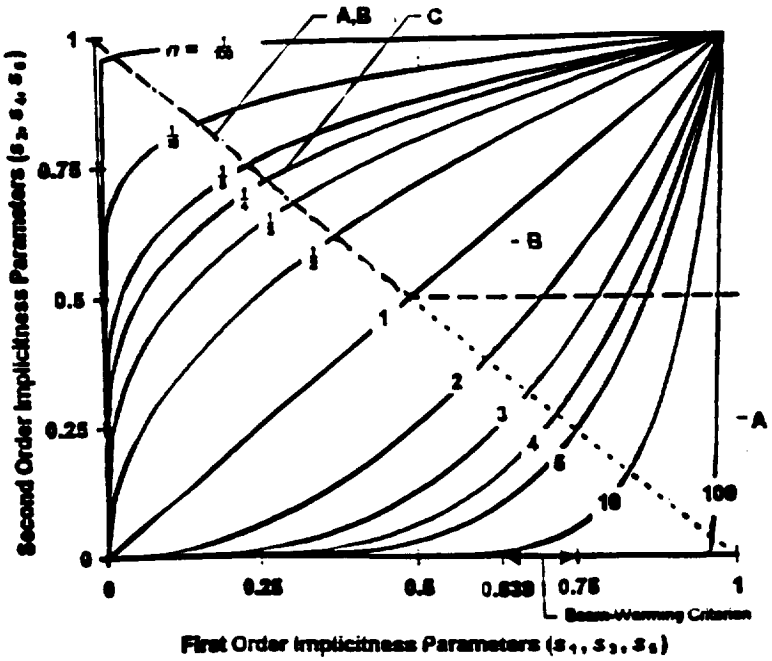

A. $s_2 = 1 - s_1, s_4 = 1 - s_3, s_6 = 1 - s_5$

B. $s_2 = \max(1 - s_1, 0.5), s_4 = \max(1 - s_3, 0.5), s_6 = \max(1 - s_5, 0.5)$

C. $s_2 = s_1^n, s_4 = s_3^n, s_6 = s_5^n, 0 < n < 1$

Fig 3. Relationships between the first and second order implicitness parameters. Stable solutions occur in the range, $0 < n < 1$, with an optimum at $n \approx \frac{1}{4}$ for the second order implicitness parameters to preserve the solution accuracy as dictated by the first order implicitness parameters.

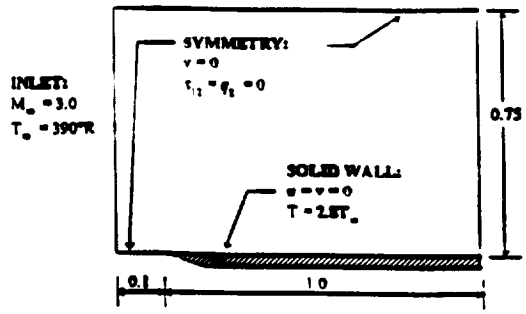

(a) Geometry and boundary conditions of Carter's [17] flat plate problem. $M_\infty = 3.$, $Re_L = 1000$, $T_\infty = 390^\circ R$

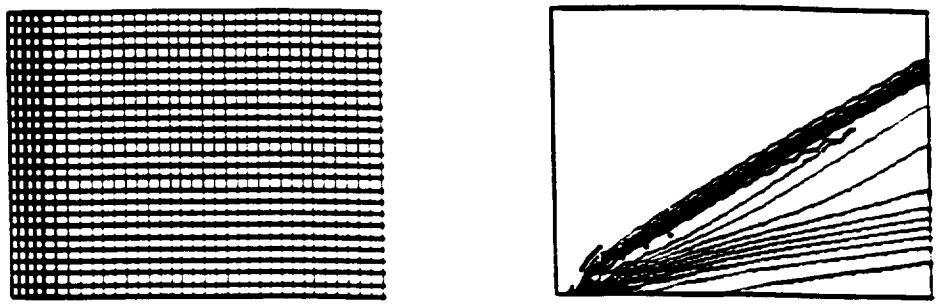

(b) Initial mesh (816 elements, 875 nodes) and the corresponding density contours, $\left(\max = 2.21\ Kg/m^3,\ \min = 0.5\ Kg/m^3\right)$

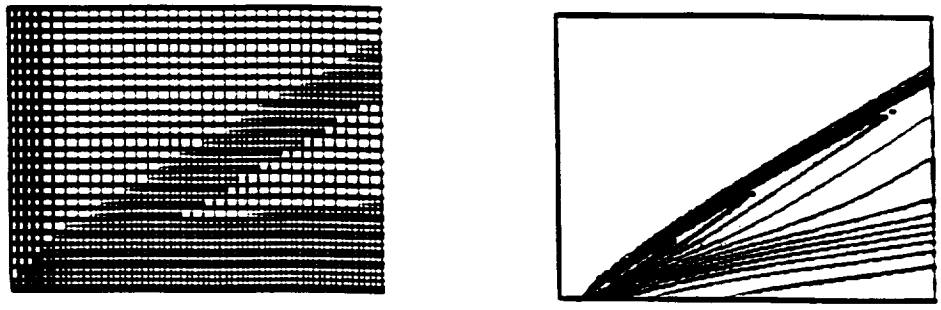

(c) One-level adaptive mesh (1755 elements, 1889 nodes) and the corresponding density contours, $\left(\max = 2.1\ Kg/m^3,\ \min = 0.5\ Kg/m^3\right)$

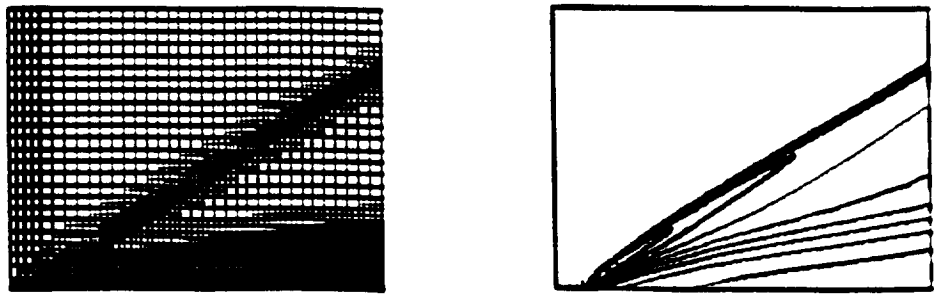

(d) Two-level adaptive mesh (4257 elements, 4547 nodes) and the corresponding density contours, $\left(\max = 2.0\ Kg/m^3,\ \min = 0.5\ Kg/m^3\right)$

Fig. 4 Flat plate problem - initial and adaptive meshes and their corresponding density contours

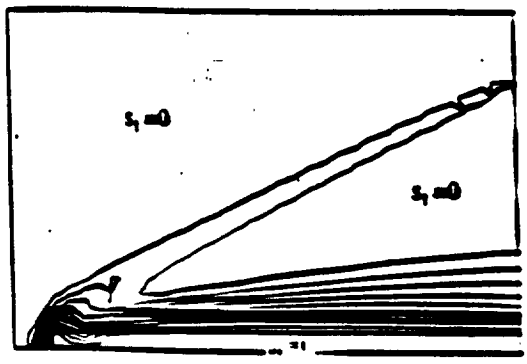

(a) s_1 contours

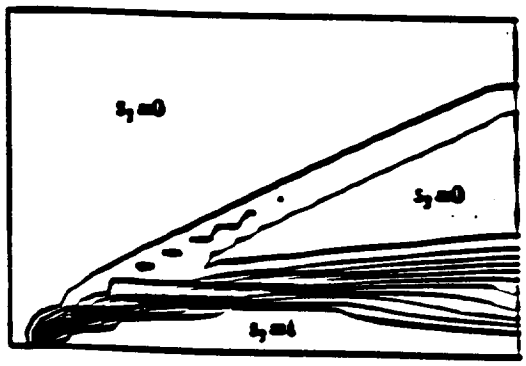

(b) s_3 contours

Fig. 5 Flowfield-dependent first order convection and diffusion implicitness parameters

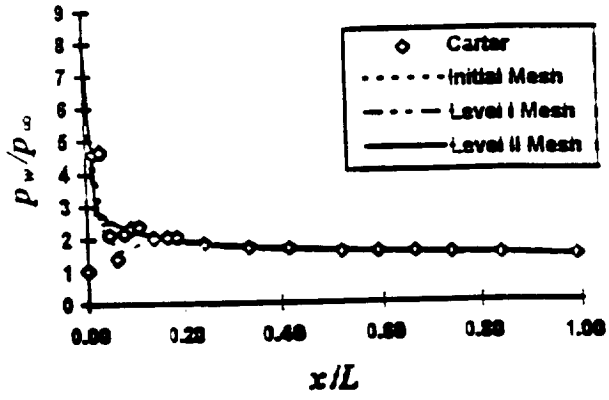

(a) Wall pressure

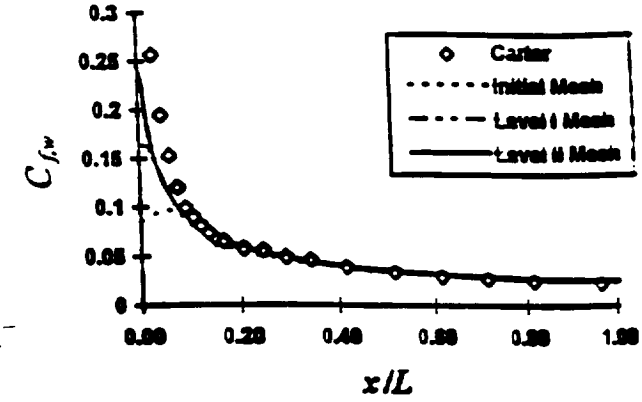

(b) Wall skin friction

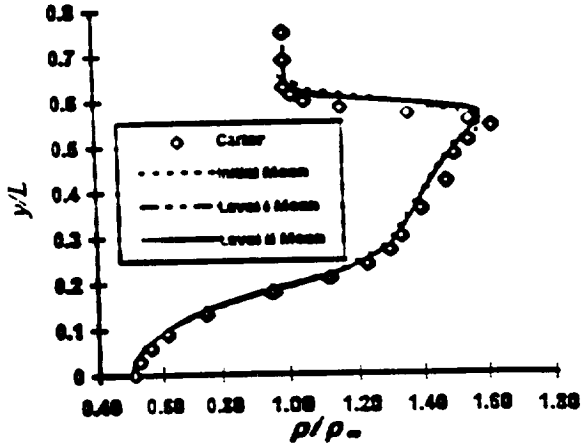

(c) Density distribution, $x/L = 1$

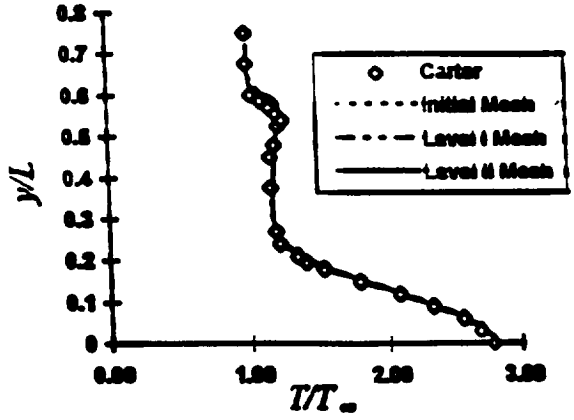

(d) Temperature distribution, $x/L = 1$

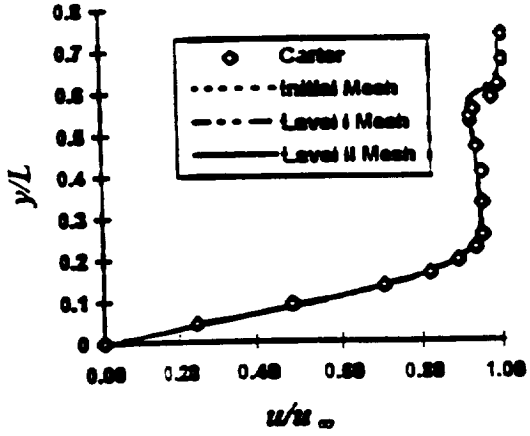

(e) u-velocity, $x/L = 1$

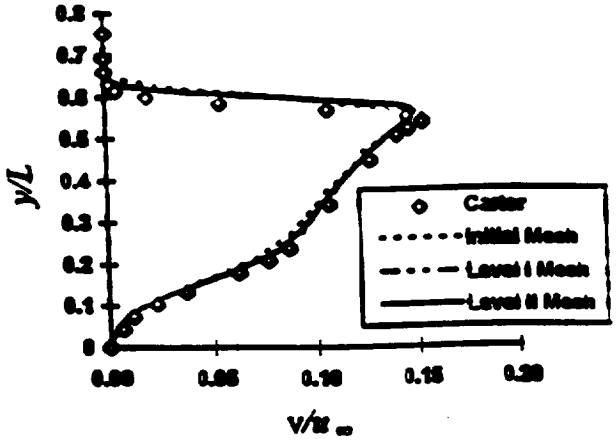

(f) v-velocity, $x/L = 1$

Fig. 6 Comparisons of various quantities with Carter [17]

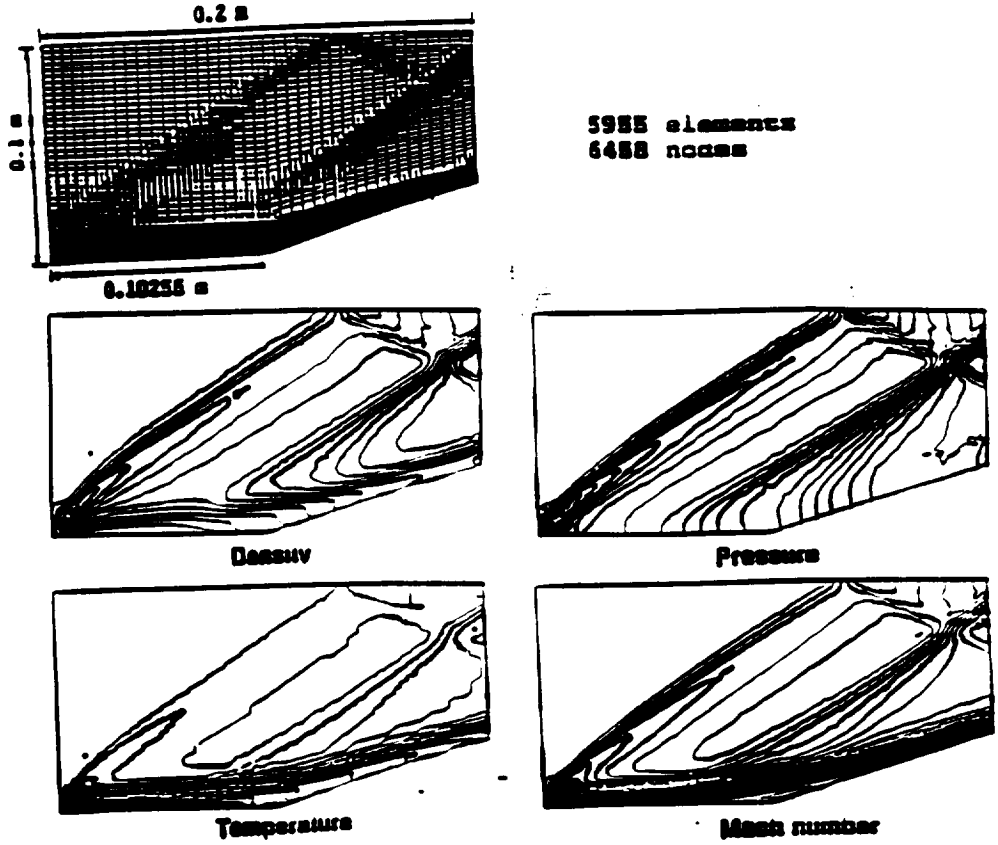

(a) Compression corner geometry and flowfields

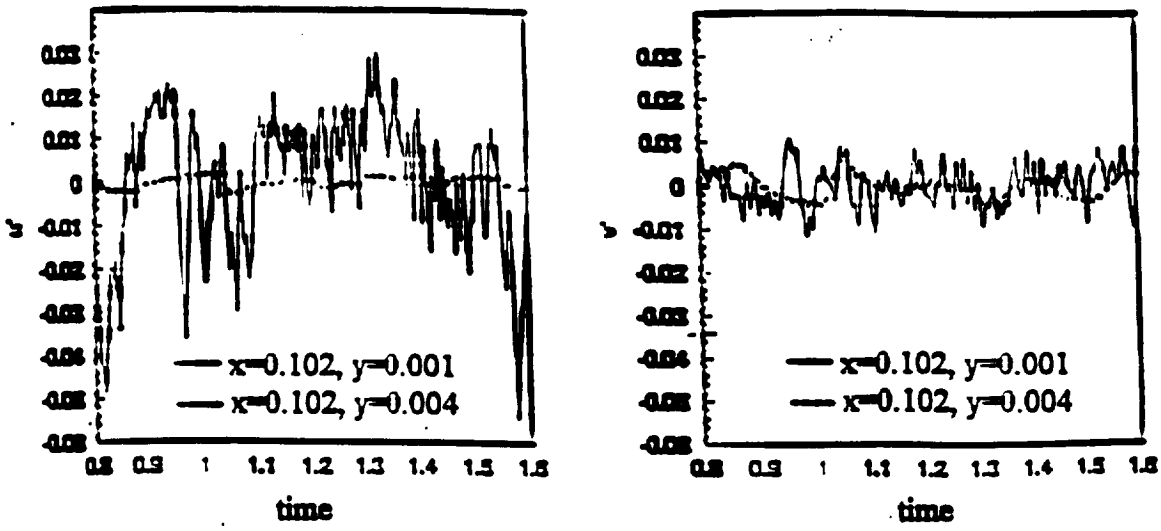

(b) Fluctuation velocities

Fig. 7 Supersonic Flow on a Compression Corner, $M_\infty = 2.25$

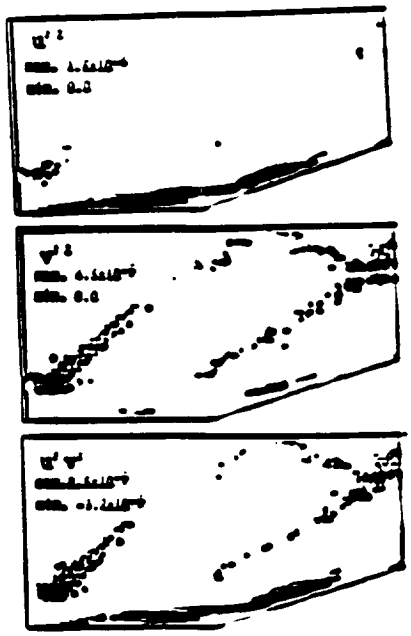

(c) Reynoids stresses

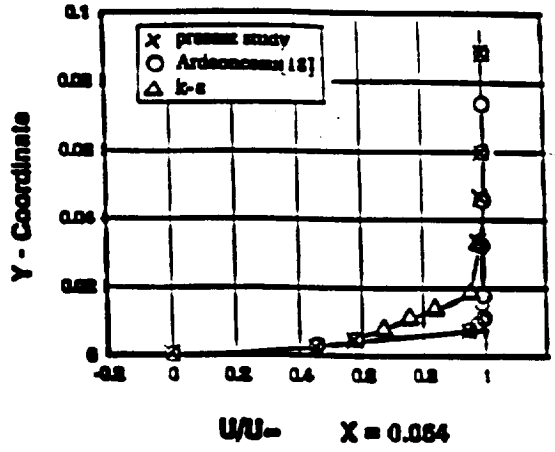

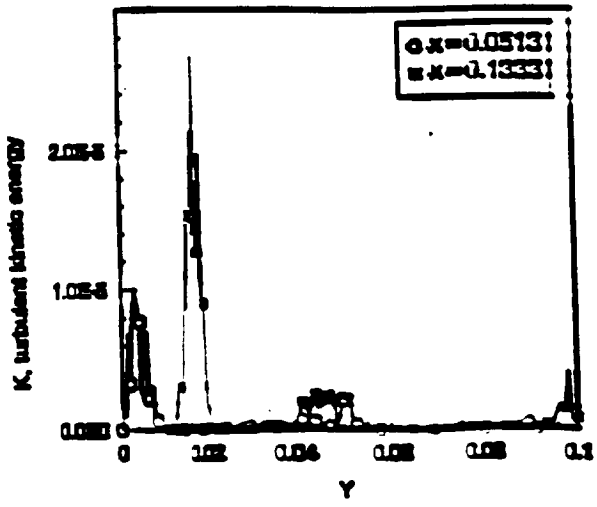

(d) Turbulent kinetic energy

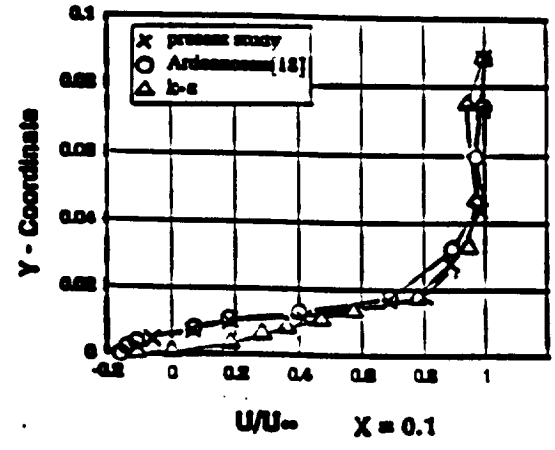

(e) Comparison velocity distribution of FDMEI with k-ε model and experimental data [18]

Fig. 7 Continued

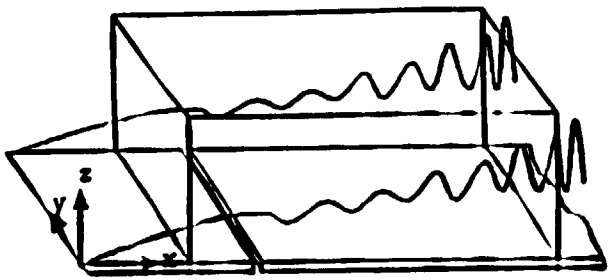

(a) Schematics of spatially evolving boundary layer flow

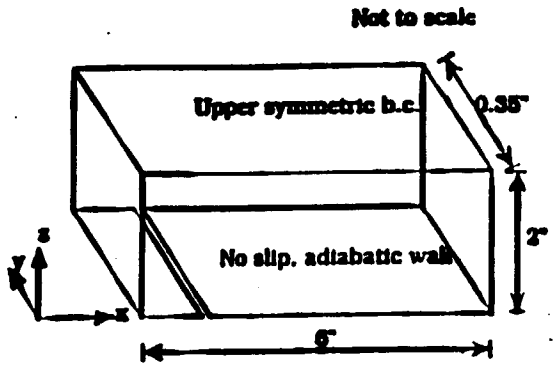

(b) Computational geometry and boundary conditions

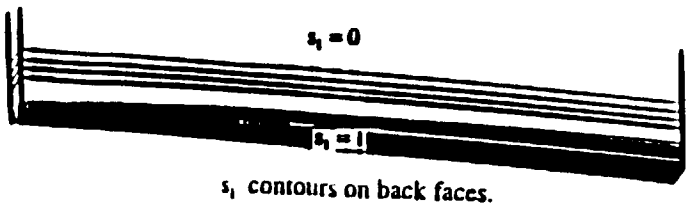

s_1 contours on back faces.

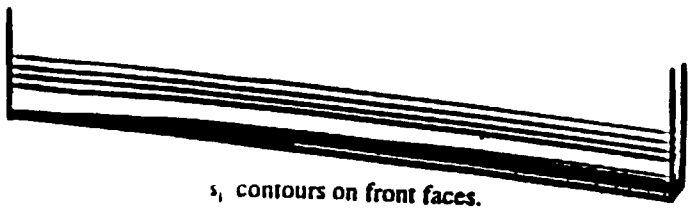

s_1 contours on front faces.

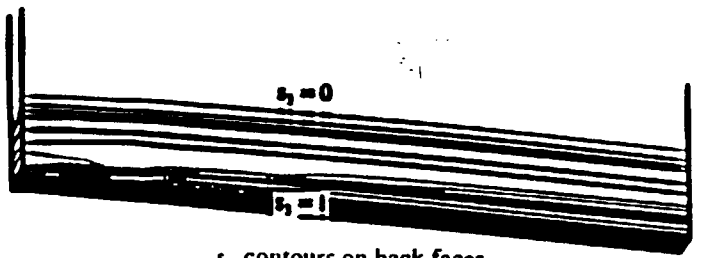

s_2 contours on back faces.

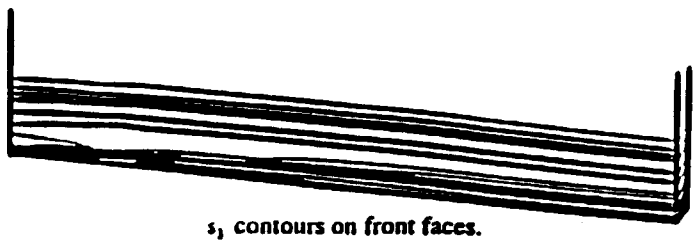

s_2 contours on front faces.

(c) Flowfield-dependent first order convection and diffuison implicitness parameter contours

Fig. 8 Three-dimensional Spatially evolving boundary layer flow

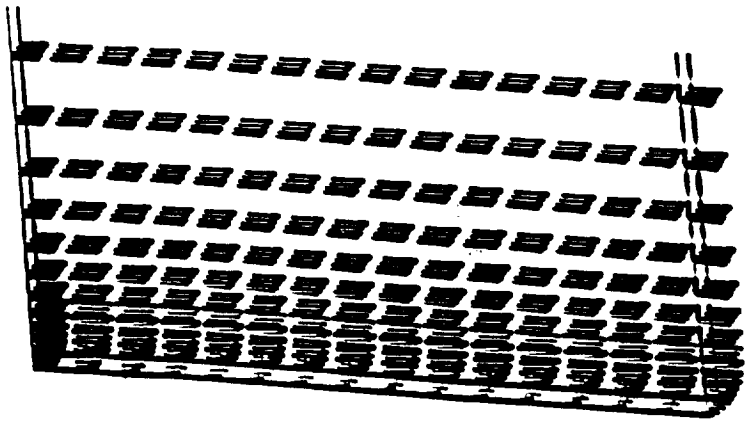

(d) Velocity vectors

Fig. 21 Velocity vectors (magnified ten fold in a vertical direction).

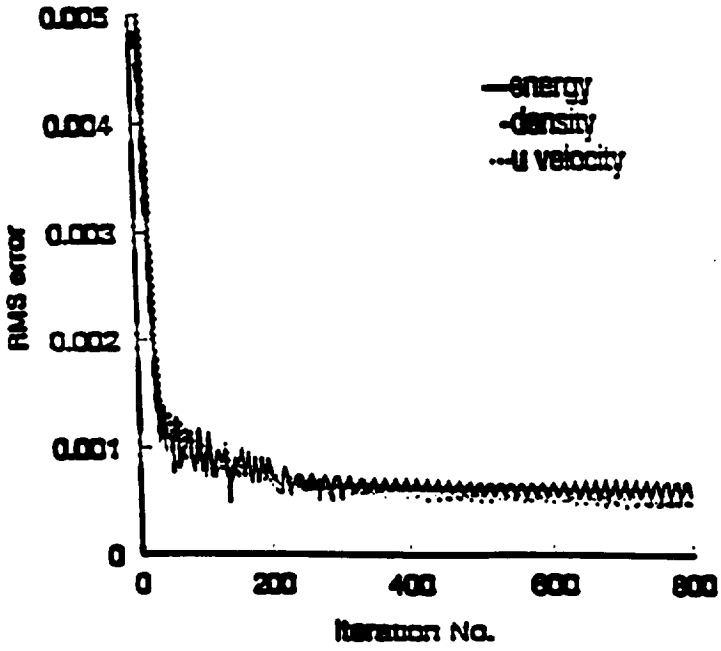

(e) Convergence history

Fig. 8 Continued

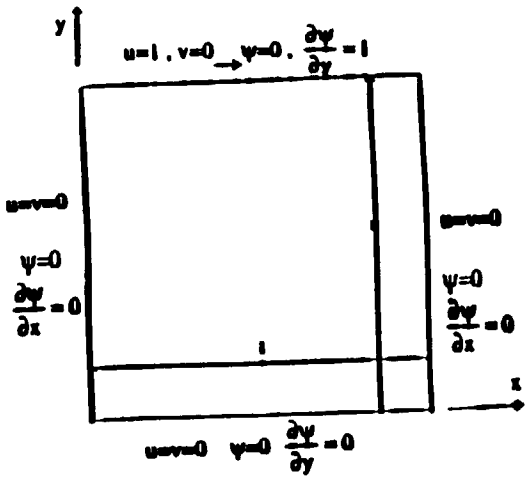

(a) Geometry and boundary conditions

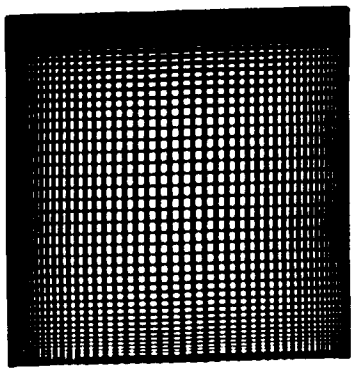

(b) Mesh configuration

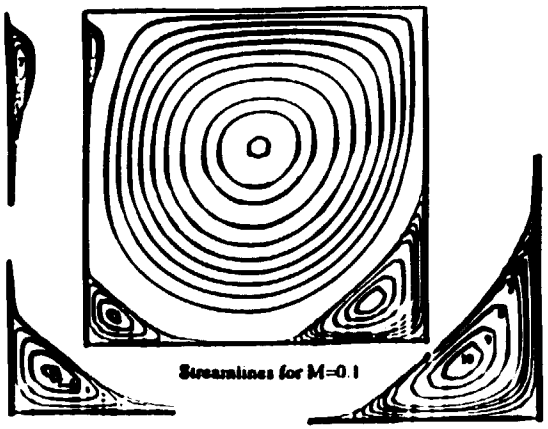

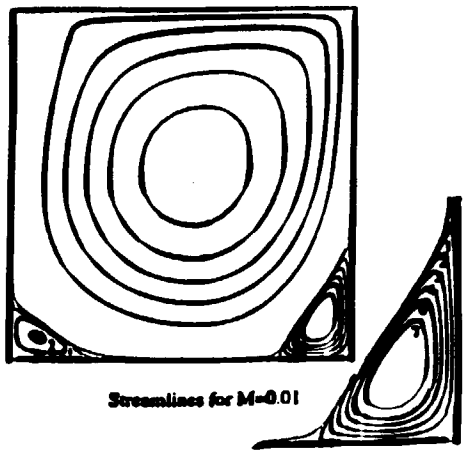

(c) Streamline Contours

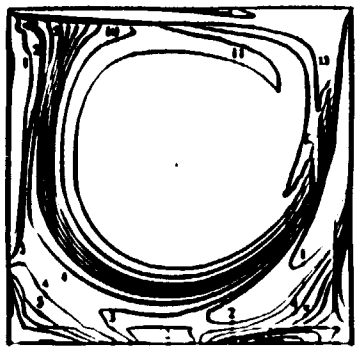

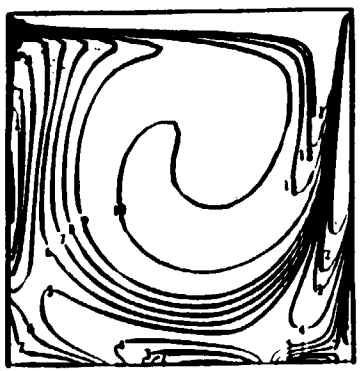

(d) Vorticity Contours

Fig. 9 Test of FDMHI Scheme to solve incompressible flows-lid-driven cavity problem

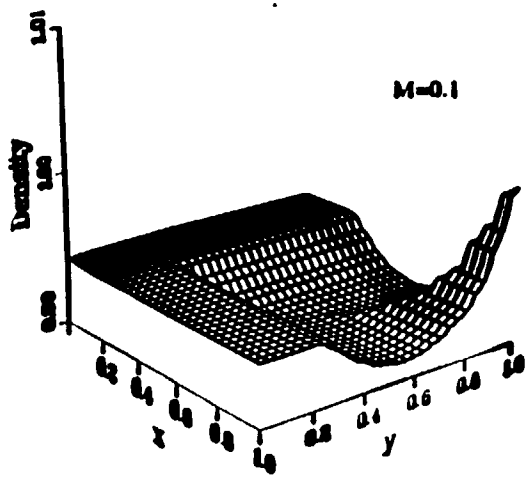

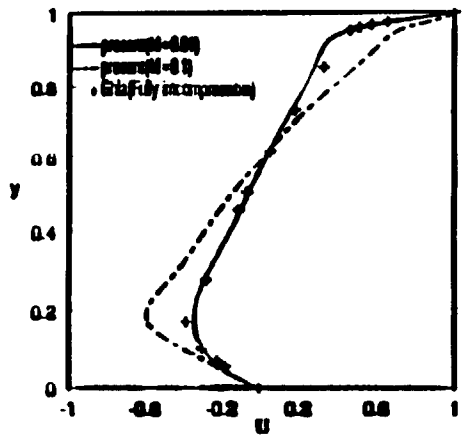

u-velocity profile along the vertical line through geometric center.

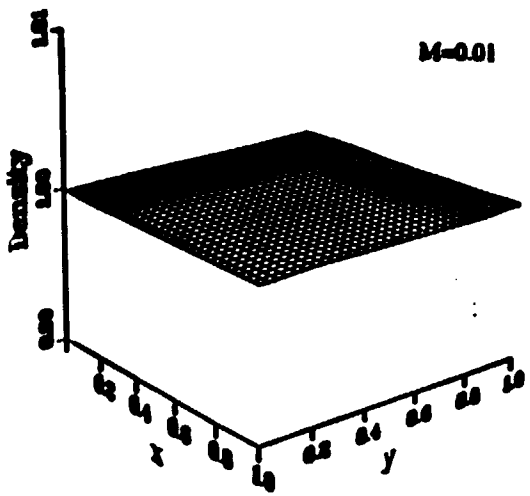

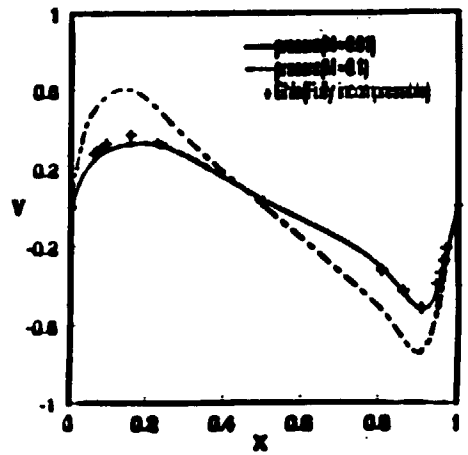

v-velocity profile along the horizontal line through geometric center.

(e) Density distribution

(f) *u*-and v-velocity comparisons with Ghia et. al. [19]

Fig. 9 Continued

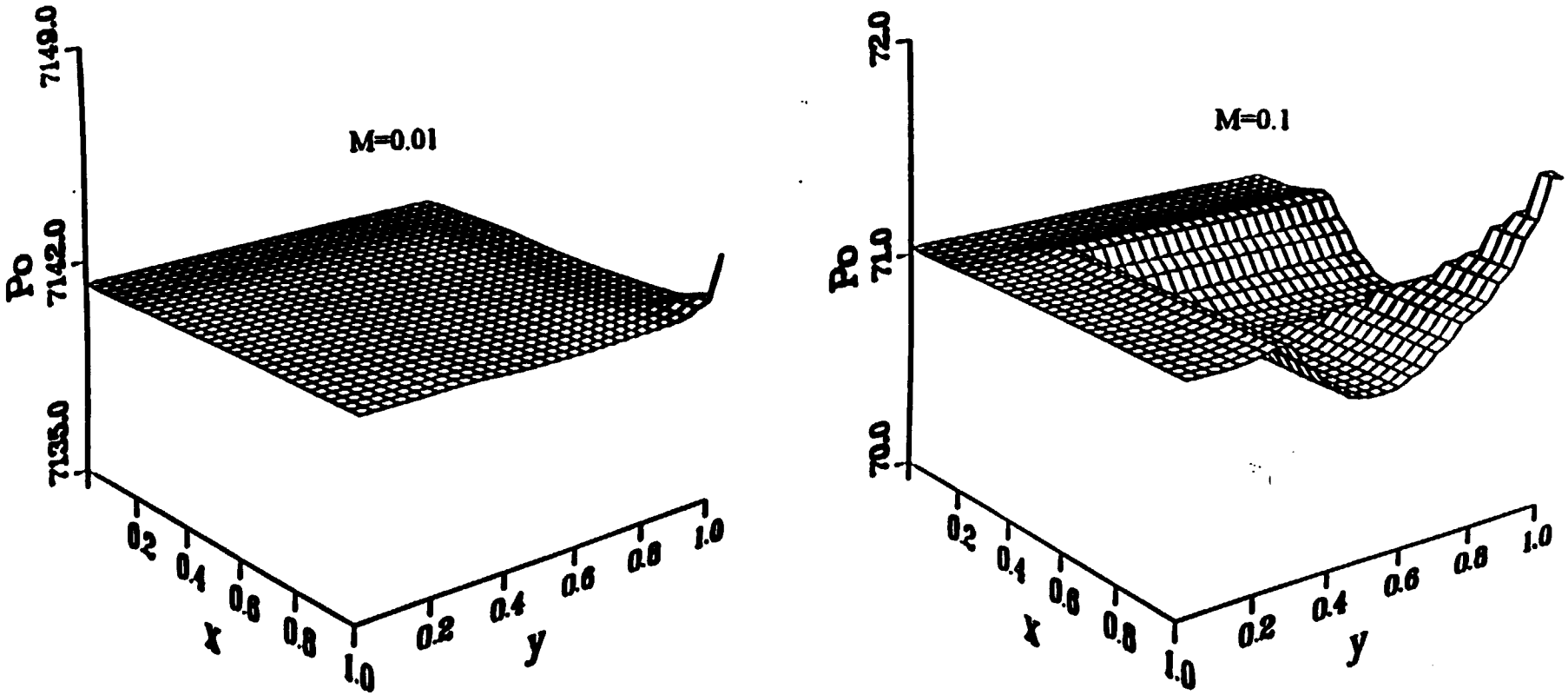

(g) Stagnation pressure at M=0.01 and M=0.1

Fig. 9 Continued

APPENDIX A

ANALOGIES OF FDMEI TO CURRENTLY AVAILABLE FDM AND FEM SCHEMES

Analogies of FDMEI to currently available computational schemes of FDM and FEM are summarized below.

A1. Analogies of FDMEI to FDM

Some of the FDM schemes are compared with FDMEI in the following Table.

	s_1	s_3	E_i	E_{ij}	Q^n	Truncation error
Beam-Warming [1]	$\frac{\theta}{1+\xi}$	$\frac{\theta}{1+\xi}$	$\frac{\theta\Delta t}{1+\xi}(\mathbf{a}_i+\mathbf{b}_i)$	$\frac{\theta\Delta t}{1+\xi}\mathbf{c}_{ij}$	$\frac{\Delta t}{1+\xi}\mathbf{W}^n+\frac{\xi}{1+\xi}\Delta\mathbf{U}^n$	$O\left[(\theta-\frac{1}{2}-\xi)\Delta t^2,\Delta t^3\right]$
Euler explicit	0	0	"	"	"	$O(\Delta t^2)$
Euler implicit	1	1	"	"	"	$O(\Delta t^2)$
Three-point implicit	$\frac{2}{3}$	$\frac{2}{3}$	"	"	"	$O(\Delta t^3)$
Trapezoidal implicit	$\frac{1}{2}$	$\frac{1}{2}$	"	"	"	$O(\Delta t^3)$
Leap frog explicit	0	0	"	"	"	$O(\Delta t^3)$

Other schemes of FDM are compared with FDMEI as follows:

(a) ***Lax-Wendroff Scheme***

The Lax-Wendroff scheme without artificial viscosity takes the form

$$\Delta\mathbf{U}_i^{n+1}=-\frac{\Delta t}{\Delta x}\left(\mathbf{F}_{i+\frac{1}{2}}-\mathbf{F}_{i-\frac{1}{2}}\right)-\frac{\Delta t}{2\Delta x^2}\left[\mathbf{a}_{i+\frac{1}{2}}\mathbf{F}_{i+1}-\left(\mathbf{a}_{i+\frac{1}{2}}-\mathbf{a}_{i-\frac{1}{2}}\right)\mathbf{F}_i+\mathbf{a}_{i-\frac{1}{2}}\mathbf{F}_{i-1}\right] \tag{A1}$$

This scheme arises if we set in FDMEI

$$\mathbf{a}_{i+\frac{1}{2}}=\mathbf{a}_{i-\frac{1}{2}}=\mathbf{a}\quad,\quad s_1=0\quad,\quad s_2=0\quad,\quad s_3=0\quad,\quad s_4=0$$

(b) ***Lax-Wendroff Scheme with Viscosity***

The Lax-Wendroff scheme with viscosity is given by

$$\Delta \mathbf{U}_i^{n+1} = -\frac{\Delta t}{\Delta x}\left(\mathbf{F}^*_{i+\frac{1}{2}} - \mathbf{F}^*_{i-\frac{1}{2}}\right) \tag{A2}$$

with

$$\mathbf{F}^*_{i+\frac{1}{2}} = \frac{\mathbf{F}_{i+1} + \mathbf{F}_i}{2} - \frac{\Delta t}{2\Delta x}\mathbf{a}_{i+\frac{1}{2}}\left(\mathbf{F}_{i+1} - \mathbf{F}_i\right) + D_{i+\frac{1}{2}}\left(\mathbf{U}_{i+1} - \mathbf{U}_i\right)$$

$$\mathbf{F}^*_{i-\frac{1}{2}} = \frac{\mathbf{F}_i + \mathbf{F}_{i-1}}{2} - \frac{\Delta t}{2\Delta x}\mathbf{a}_{i-\frac{1}{2}}\left(\mathbf{F}_i - \mathbf{F}_{i-1}\right) + D_{i-\frac{1}{2}}\left(\mathbf{U}_i - \mathbf{U}_{i-1}\right)$$

This scheme arises if we set

$$D_{i+\frac{1}{2}} = D_{i-\frac{1}{2}} = \mathbf{a}s_1 \quad , \quad s_2 = 0 \quad , \quad s_3 = 0 \quad , \quad s_4 = 0$$

This implies that $\mathbf{a}s_1$ in FDMEI plays a role of artificial viscosity which is manually implemented in the Lax-Wendroff scheme.

(c) ***Explicit McCormack Scheme***

Combining the predictor corrector steps of McCormack scheme we write

$$\begin{aligned}
\Delta \mathbf{U}_i^{n+1} &= -\frac{\Delta t}{\Delta x}\left(\mathbf{F}^n_{i+1} - \mathbf{F}^n_i\right) - \frac{\Delta t}{\Delta x}\left(\mathbf{F}^*_i - \mathbf{F}^*_{i-1}\right) + D_i \\
&= -\frac{\Delta t}{\Delta x}\left(\mathbf{F}^n_{i+1} - \mathbf{F}^n_i\right) - \frac{\Delta t}{\Delta x}\left(\mathbf{F}_{i+\frac{1}{2}} - \mathbf{F}_{i-\frac{1}{2}}\right) \\
&\quad -\frac{\Delta t}{\Delta x^2}\left[\mathbf{a}_{i+\frac{1}{2}}\mathbf{F}_{i+1} - \left(\mathbf{a}_{i+\frac{1}{2}} + \mathbf{a}_{i-\frac{1}{2}}\right)\mathbf{F}_i + \mathbf{a}_{i-\frac{1}{2}}\mathbf{F}_{i-1}\right] + D_i
\end{aligned} \tag{A3}$$

The FDMEI becomes identical to this scheme with the following adjustments:

$$\mathbf{a}_{i+\frac{1}{2}} = \mathbf{a}_{i-\frac{1}{2}} = \mathbf{a}$$

$$\mathbf{F}^n_i - \mathbf{F}^n_{i-1} = \mathbf{F}^n_{i+1} - \mathbf{F}^n_i + \mathbf{F}_{i+\frac{1}{2}} - \mathbf{F}_{i-\frac{1}{2}}$$

$$s_1 = 0 \quad , \quad s_2 = 0 \quad , \quad s_3 = 0 \quad , \quad s_4 = 0$$

and the s_2 term in the FDMEI method is equivalent to

$$D_i = \frac{\omega}{8}\left(\mathbf{U}^n_{i+\frac{1}{2}} - 4\mathbf{U}^n_{i+1} + 6\mathbf{U}^n_i - 4\mathbf{U}^n_{i-1} + \mathbf{U}^n_{i-2}\right)$$

This again is a manifestation that shows the equivalent of the s_2 terms is manually supplied in the McCormack method.

(d) ***First Order Upwind Scheme***

This scheme is written as

$$\begin{aligned}\Delta \mathbf{U}_i^{n+1} &= -\frac{\Delta t}{\Delta x}\left(\mathbf{F}^*_{i+\frac{1}{2}} - \mathbf{F}^*_{i-\frac{1}{2}}\right) \\ &= -\frac{\Delta t}{\Delta x}\left\{\left[\frac{1}{2}\left(\mathbf{F}_i^n + \mathbf{F}_{i+1}^n\right) - \frac{1}{2}|\mathbf{a}|\left(\mathbf{U}_{i+1}^n - \mathbf{U}_i^n\right)\right]\right. \\ &\quad \left. -\left[\frac{1}{2}\left(\mathbf{F}_i^n + \mathbf{F}_{i-1}^n\right) - \frac{1}{2}|\mathbf{a}|\left(\mathbf{U}_i^n - \mathbf{U}_{i-1}^n\right)\right]\right\}\end{aligned} \tag{A4}$$

The FDMEI analogy is obtained by setting

$$\mathbf{F}_i^n = \frac{1}{2}\mathbf{F}_{i+1}^n \quad , \quad \mathbf{F}_{i-1}^n = \frac{1}{2}\mathbf{F}_{i-1}^n$$

$$s_2 \mathbf{a} C\left(\Delta \mathbf{U}_i^{n+1} - 2\Delta \mathbf{U}_{i-1}^{n+1} + \Delta \mathbf{U}_{i-2}^{n+1}\right) = |\mathbf{a}|\left(\mathbf{U}_{i+1}^n - \mathbf{U}_{i-1}^n\right)$$

where C is the Courant number.

(e) ***Implicit McCormack Scheme***

With all second order derivatives removed from (11) we obtain the implicit McCormack Scheme by setting $s_1 = 1$, $s_2 = 0$, $s_3 = 0$, $s_4 = 0$. However, it is necessary to divide the process into the predictor and corrector steps. Once again the flowfield-dependent implicitness parameters for FDMEI will allow the computation to be performed in a single step.

(f) ***PISO and SIMPLE***

The basic idea of PISO and SIMPLE is analogous to FDMEI-FEM in that the pressure correction process is a separate step in PISO or SIMPLE, whereas the concept of pressure correction is implicitly embedded in FDMEI-FEM by updating the implicitness parameters based on the upstream and downstream Mach numbers and Reynolds numbers within an element.

The elliptic nature of the pressure Poisson equation in the pressure correction process resembles the terms embedded in the $B_{\alpha\beta rs}$ terms in (28a). Specifically, examine the s_2 terms involving $a_{irq}\, a_{jsq}$ and $b_{irq} a_{jsq}$ and s_4 term involving $a_{irq} b_{jsq}$. All of these terms are multiplied by $\Phi_{\alpha i}$ $\Phi_{\beta j}$ which provide dissipation against any pressure oscillations. Question: Exactly when is such dissipation action needed? This is where the importance of implicitness parameters based on flowfield parameters comes in. As the Mach number becomes very small (incompressibility effects dominate) the implicitness parameters s_2 and s_4 calculated from the current flowfield will be indicative of pressure correction required. Notice that a delicate balance between Mach number (s_2 is Mach number dependent) and Reynolds number or Peclet number (s_4 is Reynolds number or Peclet number dependent) is a crucial factor in achieving a convergent and stable solutions. Of course, on the other hand, high Mach number flows are also dependent on these implicitness parameters. In this case all implicitness parameters, s_1, s_2, s_3, s_4 will play important roles.

A2. Analogies of FDMEI to FEM

(a) *Generalized Taylor Galerkin (GTG) with Convection and Diffusion Jacobians*

Earlier developments for the solution of Navier-Stokes system of equations were based on GTG without using the implicitness parameters. They can be shown to be special cases of FDMEI-FEM.

In terms of both diffusion Jacobian and diffusion gradient Jacobian, we write

$$\frac{\partial \mathbf{G}_i}{\partial t} = \mathbf{b}_i \frac{\partial \mathbf{U}}{\partial t} + \mathbf{c}_{ij} \frac{\partial \mathbf{V}_j}{\partial t}$$

with

$$\mathbf{b}_i = \frac{\partial \mathbf{G}_i}{\partial \mathbf{U}} \quad , \quad \mathbf{c}_{ij} = \frac{\partial \mathbf{G}_i}{\partial \mathbf{V}_j} \quad , \quad \mathbf{V}_j = \frac{\partial \mathbf{U}}{\partial x_j}$$

Thus it follows from (10) or (11) with $s_1 = s_3 = s_4 = s_5 = s_6 = 0$ and $s_2 = 1$ that

$$\Delta \mathbf{U}^{n+1} = \Delta t \left(-\frac{\partial \mathbf{F}_i}{\partial x_i} - \frac{\partial \mathbf{G}_i}{\partial x_i} + \mathbf{B} \right)^n + \frac{\Delta t^2}{2} \frac{\partial}{\partial t} \left(-\frac{\partial \mathbf{F}_i}{\partial x_i} - \frac{\partial \mathbf{G}_i}{\partial x_i} + \mathbf{B} \right)^{n+1} + O\left(\Delta t^3\right) \tag{A5}$$

Using the definitions of convection, diffusion, and diffusion rate Jacobians discussed in Section 2, the temporal rates of change of convection and diffusion variables may be written as follows:

$$\frac{\partial \mathbf{F}_i^n}{\partial t} = \left(\mathbf{a}_i \frac{\partial \mathbf{U}}{\partial t} \right)^n = \left[\mathbf{a}_i \left(-\frac{\partial \mathbf{F}_j}{\partial x_j} - \frac{\partial \mathbf{G}_j}{\partial x_j} + \mathbf{B} \right) \right]^n$$

$$\frac{\partial \mathbf{F}_i^{n+1}}{\partial t} = \mathbf{a}_i \left[\left(-\mathbf{a}_j \frac{\partial}{\partial x_j} \left(\mathbf{U}^{n+1} - \mathbf{U}^n \right) - \frac{\partial \mathbf{F}_j^n}{\partial x_j} - \frac{\partial \mathbf{G}_j^{n+1}}{\partial x_j} + \mathbf{B}^{n+1} \right) \right] \tag{A6}$$

$$\frac{\partial \mathbf{G}_i^{n+1}}{\partial t} = \left(\mathbf{b}_i \frac{\partial \mathbf{U}}{\partial t} \right)^{n+1} + \left[\mathbf{c}_{ij} \frac{\partial}{\partial t} \left(\frac{\partial \mathbf{U}}{\partial x_j} \right) \right]^{n+1}$$

or

$$\frac{\partial \mathbf{G}_i^{n+1}}{\partial t} = \left(\mathbf{b}_i - \frac{\partial \mathbf{c}_{ij}}{\partial x_j} \right) \frac{\Delta \mathbf{U}}{\Delta t}^{n+1} + \frac{\partial}{\partial x_j} \left(\mathbf{c}_{ij} \frac{\Delta \mathbf{U}}{\Delta t} \right)^{n+1} \tag{A7}$$

Substituting (A6) and (A7) into (A5) yields

$$\Delta\mathbf{U}^{n+1} = \Delta t\left(-\frac{\partial \mathbf{F}_i}{\partial x_i}-\frac{\partial \mathbf{G}_i}{\partial x_i}+\mathbf{B}\right)^n+\frac{\Delta t^2}{2}\left\{\frac{\partial}{\partial x_i}\left[-\mathbf{a}_i\left(-\mathbf{a}_j\frac{\partial \Delta\mathbf{U}^{n+1}}{\partial x_j}-\frac{\partial \mathbf{F}_j^n}{\partial x_j}-\frac{\partial \mathbf{G}_j^{n+1}}{\partial x_j}+\mathbf{B}^{n+1}\right)\right.\right.$$
$$\left.\left.+\left(\mathbf{e}_i+\frac{\partial \mathbf{c}_{ij}}{\partial x_j}\right)\frac{\Delta\mathbf{U}^{n+1}}{\Delta t}+\frac{\partial \mathbf{B}^{n+1}}{\partial t}\right]\right\} \tag{A8}$$

Assuming that

$$\mathbf{e}_i = \mathbf{b}_i - \frac{\partial \mathbf{c}_{ij}}{\partial x_j} \equiv 0$$

and neglecting the spatial and temporal derivatives of **B**, we rewrite (A8) in the form

$$\left\{1-\frac{\Delta t^2}{2}\frac{\partial}{\partial x_i}\left(\mathbf{a}_i\mathbf{a}_j+\frac{\mathbf{c}_{ij}}{\Delta t}\right)\frac{\partial}{\partial x_j}\right\}\Delta\mathbf{U}^{n+1} = \mathbf{H}^n \tag{A9}$$

$$\mathbf{H}^n = \Delta t\left(-\frac{\partial \mathbf{F}_i}{\partial x_i}-\frac{\partial \mathbf{G}_i}{\partial x_i}+\mathbf{B}\right)^n+\frac{\Delta t^2}{2}\frac{\partial}{\partial x_i}\left(\mathbf{a}_i\frac{\partial \mathbf{F}_j}{\partial x_j}\right)^n$$

Here the second derivatives of $\mathbf{G}_i$ are neglected and all Jacobians are assumed to remain constant within an incremental time step but updated at subsequent time steps.

Applying the Galerkin finite element formulation, we have an implicit scheme,

$$\left(\mathbf{A}_{\alpha\beta}\delta_{rs}+\mathbf{B}_{\alpha\beta rs}\right)\Delta\mathbf{U}_{\beta s}^{n+1} = \mathbf{H}_{\alpha r}^n+\mathbf{N}_{\alpha r}^{n+1}+\mathbf{N}_{\alpha r}^n \tag{A10}$$

where

$$\mathbf{B}_{\alpha\beta rs} = \frac{\Delta t^2}{2}\int_\Omega\left[\left(\mathbf{a}_{irq}\mathbf{a}_{jsq}+\frac{\mathbf{c}_{ijrs}}{\Delta t}\right)\Phi_{\alpha,i}\Phi_{\beta,j}\right]d\Omega$$

$$\mathbf{H}_{\alpha r}^n = \Delta t\int_\Omega\left[\Phi_{\alpha,i}\Phi_\beta\left(\mathbf{F}_{\beta ir}^n+\mathbf{G}_{\beta ir}^n\right)-\Phi_\alpha\Phi_\beta\mathbf{B}_{\beta r}^n-\frac{\Delta t^2}{2}\mathbf{a}_{irs}\Phi_{\alpha,i}\Phi_{\beta,j}\mathbf{F}_{\beta js}^n\right]d\Omega$$

$$\mathbf{N}_{\alpha r}^{n+1} = \frac{\Delta t^2}{2}\int_\Gamma\left(\mathbf{a}_{irq}\mathbf{a}_{jsq}+\frac{\mathbf{c}_{ijrs}}{\Delta t}\right)\dot{\Phi}_\alpha\,\Delta\mathbf{U}_{s,j}^{n+1}n_i d\Gamma$$

$$\mathbf{N}_{\alpha r}^n = -\int_\Gamma\left[\Delta t\,\dot{\Phi}_\alpha\left(\mathbf{F}_{ir}^n+\mathbf{G}_{ir}^n\right)-\frac{\Delta t^2}{2}\mathbf{a}_{irs}\dot{\Phi}_\alpha\mathbf{F}_{js,j}^n\right]n_i d\Gamma$$

Here we note that the algorithm given by (A10) results from (29) by setting

$s_1 = s_3 = s_4 = 0$, $s_2 = 1$, $b_{irq}a_{jsq} = c_{ijrs}/\Delta t$, and neglecting the terms with b_{jrs} and derivatives of $\mathbf{G}_i$ and $\mathbf{B}$, the form identical to that reported by Hassan et al [13].

(b) *GTG With Convection Jacobians*

Diffusion Jacobians may be neglected if their influences is negligible. In this case the Taylor-Galerkin finite element analog may be derived using only the convective Jacobian from the Taylor series expansion,

$$\mathbf{U}^{n+1} = \mathbf{U}^n + \Delta t\frac{\partial \mathbf{U}^n}{\partial t} + \frac{\Delta t^2}{2}\frac{\partial^2 \mathbf{U}^n}{\partial t^2} + O\left(\Delta t^3\right) \tag{A11}$$

where

$$\frac{\partial \mathbf{U}}{\partial t} = -\frac{\partial \mathbf{F}_i}{\partial x_i} - \frac{\partial \mathbf{G}_i}{\partial x_i} + \mathbf{B} = -\mathbf{a}_i\frac{\partial \mathbf{U}}{\partial x_i} - \frac{\partial \mathbf{G}_i}{\partial x_i} + \mathbf{B} \tag{A12}$$

$$\frac{\partial^2 \mathbf{U}}{\partial t^2} = -\frac{\partial}{\partial t}\left(\mathbf{a}_i\frac{\partial \mathbf{U}}{\partial x_i} + \frac{\partial \mathbf{G}_i}{\partial x_i} - \mathbf{B}\right)$$

or

$$\frac{\partial^2 \mathbf{U}}{\partial t^2} = \frac{\partial}{\partial x_j}\left(\mathbf{a}_i\mathbf{a}_j\frac{\partial \mathbf{U}}{\partial x_i}\right) + \frac{\partial}{\partial x_i}\left(\mathbf{a}_i\frac{\partial \mathbf{G}_j}{\partial x_j}\right) - \frac{\partial}{\partial x_i}(\mathbf{a}_i\mathbf{B}) + \frac{\partial \mathbf{B}}{\partial t} \tag{A13}$$

Substituting (A12) and (A13) into (A11), we obtain

$$\Delta \mathbf{U}^{n+1} = \Delta t\left\{-\frac{\partial \mathbf{F}_i}{\partial x_i} - \frac{\partial \mathbf{G}_i}{\partial x_i} + \mathbf{B} + \frac{\Delta t}{2}\left[\frac{\partial}{\partial x_j}\left(\mathbf{a}_i\mathbf{a}_j\frac{\partial \mathbf{U}}{\partial x_i}\right) + \frac{\partial^2(\mathbf{a}_i\mathbf{G}_j)}{\partial x_i\partial x_j} + \frac{\partial}{\partial x_i}(\mathbf{a}_i\mathbf{B}) + \frac{\partial \mathbf{B}}{\partial t}\right]\right\}^n \tag{A14a}$$

Expanding $\partial \mathbf{F}_j/\partial t$ at $(n+1)$ time step

$$\frac{\partial \mathbf{F}_i^{n+1}}{\partial t} = \left[\mathbf{a}_i\left(-\frac{\partial \mathbf{F}_j}{\partial x_j} - \frac{\partial \mathbf{G}_j}{\partial x_j} + \mathbf{B}\right)\right]^{n+1} = \mathbf{a}_i^{n+1}\left[-\mathbf{a}_j\frac{\partial \Delta \mathbf{U}^{n+1}}{\partial x_j} - \frac{\partial \mathbf{F}_j^n}{\partial x_j} - \frac{\partial \mathbf{G}_j^{n+1}}{\partial x_j} + \mathbf{B}^{n+1}\right]$$

and substituting the above into (A11 - A13), we arrive at $\Delta \mathbf{U}^{n+1}$ in a form different from (A14a),

(d) *Characteristic-Based Zienkiewics/Codina Scheme*

This scheme arises from Eq. (10) by splitting the FDMEI Navier-Stokes system of equations into three parts for continuity, momentum, and energy, separately.

Continuity

$$\Delta \mathbf{U}^{n+1} = -\Delta t \left[\frac{\partial \mathbf{F}_i^n}{\partial x_i} + s_1 \frac{\partial \mathbf{a}_i \Delta \mathbf{U}^{n+1}}{\partial x_i} - \frac{\Delta t}{2} \left(\frac{\partial^2 \mathbf{a}_i \mathbf{F}_j^n}{\partial x_i \partial x_j} + s_2 \frac{\partial^2 \mathbf{a}_i \mathbf{a}_j \Delta \mathbf{U}^{n+1}}{\partial x_i \partial x_j} \right) \right] \tag{A21}$$

where all diffusion terms are neglected. Setting

$$\begin{aligned} \Delta \mathbf{U}^{n+1} &\rightarrow \Delta \rho^{n+1} \\ \mathbf{F}_i^n &\rightarrow \rho \mathrm{v}_i^n \rightarrow U_i^n \\ s_1 \mathbf{a}_i \Delta \mathbf{U}^{n+1} &\rightarrow s_1 \Delta \rho \mathrm{v}_i^n \rightarrow \theta_1 \Delta \tilde{U}_i^n \\ \tfrac{1}{2} \mathbf{a}_i \mathbf{F}_j^n &\rightarrow \theta_1 p^n \delta_{ij} \\ \tfrac{1}{2} s_2 \mathbf{a}_i \mathbf{a}_j \Delta \mathbf{U}^{n+1} &\rightarrow \theta_1 \theta_2 \Delta p^{n+1} \delta_{ij} \end{aligned}$$

These substitutions to (A21) lead to

$$\Delta \rho^{n+1} = \left(\frac{1}{a^2} \Delta p \right)^{n+1} = -\Delta t \left[\frac{\partial (\rho \mathrm{v}_i)^n}{\partial x_i} + \theta_1 \frac{\partial (\Delta \rho \mathrm{v}_i)^{n+1}}{\partial x_i} - \Delta t \theta_1 \left(\frac{\partial^2 p^n}{\partial x_i \partial x_i} + \theta_2 \frac{\partial^2 \Delta p^{n+1}}{\partial x_i \partial x_i} \right) \right] \tag{A22}$$

which is identical to (33) with $(\Delta \rho \mathrm{v}_i)^{n+1} = \Delta \tilde{\mathbf{U}}_i^n$ being the intermediate step in [14]. This represents the pressure correction equation.

Momentum

$$\begin{aligned} (\Delta \rho \mathrm{v}_j)^{n+1} = -\Delta t & \left[\frac{\partial (\rho \mathrm{v}_i \mathrm{v}_j)^n}{\partial x_i} - \frac{\partial \tau_{ij}^n}{\partial x_i} + \frac{\partial p^n}{\partial x_j} + \theta_2 \frac{\partial \Delta p^{n+1}}{\partial x_j} \right] \\ & - (1 - \theta_2) \left[\frac{\Delta t^2}{2} \mathrm{v}_k \frac{\partial^2}{\partial x_k \partial x_i} (\rho \mathrm{v}_i \mathrm{v}_j + p \delta_{ij})^n \right] \end{aligned} \tag{A23}$$

which is similar to (30) of [14] with $\mathbf{a}_i = \mathrm{v}_i$, $1 - \theta_2 = s_1$, and all terms of s_2, $\mathbf{b}_i$, and $\mathbf{c}_{ij}$ being neglected in FDMEI.

Energy

$$(\Delta\rho E)^{n+1} = -\Delta t\left[\frac{\partial(\rho E v_i + v_i p)^n}{\partial x_i} - \frac{\partial}{\partial x_j}\left(k\frac{\partial T}{\partial x_i} + \tau_{ij} v_j\right)^n - \frac{\Delta t}{2} v_j \frac{\partial^2}{\partial x_j \partial x_i}(\rho E v_i + v_i p)^n\right] \tag{A24}$$

which is identical to (40) of [14] with all $n+1$ terms being neglected in FDMEI.

The solution steps begin with (A-23), followed by (A-21) and (A-24). Note that the pressure corrections for incompressible flows are internally carried out in FDMEI as the pressure second derivatives arise automatically in Eq(10). Note also that in FDMEI all implicit terms may be recovered if so desired.

$$\frac{\Delta \mathbf{U}}{\Delta t} + \mathbf{a}_i \frac{\partial \Delta \mathbf{U}}{\partial x_i} - \frac{\Delta t}{2} \mathbf{a}_i \mathbf{a}_j \frac{\partial^2 \Delta \mathbf{U}}{\partial x_i \partial x_j} = 0 \tag{A16}$$

For the steady state non-incremental form in 1-D we write (A16) in the form

$$a \frac{\partial u}{\partial x} - \Delta t \frac{a^2}{2} \frac{\partial^2 u}{\partial x^2} = 0 \tag{A17}$$

Taking the Galerkin integral of (A17) leads to

$$\int \Phi_N^{(e)} \left(a \frac{\partial u}{\partial x} - \Delta t \frac{a^2}{2} \frac{\partial^2 u}{\partial x^2} \right) dx = 0$$

or

$$\int W_N^{(e)} a \frac{\partial u}{\partial x} dx = 0 \tag{A18}$$

for vanishing Neumann boundaries. Here $W_N^{(e)}$ is the Petrov-Galerkin test function,

$$W_N^{(e)} = \Phi_N^{(e)} + \alpha h \frac{\partial \Phi_N^{(e)}}{\partial x} \tag{A19}$$

with $\alpha = C/2$ and $C = a\Delta t/\Delta x$ being the Courant number.

For isoparametric coordinates in two dimensions, the Petrov-Galerkin test function assumes the form

$$W_N^{(e)} = \Phi_N^{(e)} + \beta g_i \frac{\partial \Phi_N^{(e)}}{\partial x_i} \tag{A20}$$

with βg_i being the Petrov-Galerkin parameters

$$\beta = \frac{1}{4} \left(\bar{\alpha}_\xi h_\xi + \bar{\alpha}_\eta h_\eta \right)$$

$$\bar{\alpha}_\xi = \coth\left(\frac{R_\xi}{2} \right) - \frac{2}{R_\xi} \quad , \quad \bar{\alpha}_\eta = \coth\left(\frac{R_\eta}{2} \right) - \frac{2}{R_\eta}$$

$$g_i = \frac{\mathbf{v}_i}{\sqrt{\mathbf{v}_j \mathbf{v}_j}}$$

where R_ξ is the Reynolds number or Peclet number in the direction of isoparametric coordinates (ξ, η). Note that the GPG process given by (A16)-(A20) leads to the Streamline Upwinding Petrov-Galerkin (SUPG) scheme as a special case.

$$\Delta \mathbf{U}^{n+1} = \Delta t\left(-\frac{\partial \mathbf{F}_i}{\partial x_i}-\frac{\partial \mathbf{G}_i}{\partial x_i}+\mathbf{B}\right)^n+\frac{\Delta t^2}{2}\left\{\frac{\partial}{\partial x_i}\left(\mathbf{a}_i\mathbf{a}_j\frac{\partial \Delta \mathbf{U}^{n+1}}{\partial x_j}+\mathbf{a}_i\frac{\partial \mathbf{F}_j^n}{\partial x_j}\right)\right.$$
$$\left.+\frac{\partial^2\left(\mathbf{a}_i\mathbf{G}_j\right)^{n+1}}{\partial x_i\partial x_j}+\frac{\partial}{\partial x_i}\left(\mathbf{a}_i\mathbf{B}\right)^{n+1}+\frac{\partial \mathbf{B}^{n+1}}{\partial t}\right\} \tag{A 14b}$$

$$\mathbf{H}^n=\left[1-\frac{\Delta t^2}{2}\frac{\partial}{\partial x_i}\left(\mathbf{a}_i\mathbf{a}_j+\frac{\mathbf{c}_{ij}}{\Delta t}\right)\frac{\partial}{\partial x_j}\right]\Delta \mathbf{U}^{n+1} \tag{A14c}$$

$$\mathbf{H}^n=\Delta t\left(-\frac{\partial \mathbf{F}_i}{\partial x_i}-\frac{\partial \mathbf{G}_i}{\partial x_i}+\mathbf{B}\right)^n+\frac{\Delta t^2}{2}\frac{\partial}{\partial x_i}\left(\mathbf{a}_i\frac{\partial \mathbf{F}_j}{\partial x_j}\right)^n$$

where second derivatives of $\mathbf{G}_i$ is assumed to be negligible and $\mathbf{B}$ is constant in space and time, arriving at an implicit finite element scheme,

$$\left(\mathbf{A}_{\alpha\beta}\delta_{rs}+\mathbf{B}_{\alpha\beta rs}\right)\Delta \mathbf{U}_{\beta s}^{n+1}=\mathbf{H}_{\alpha r}^n+\mathbf{N}_{\alpha r}^{n+1}+\mathbf{N}_{\alpha r}^n \tag{A15}$$

where

$$\mathbf{A}_{\alpha\beta}=\int_\Omega \Phi_\alpha\Phi_\beta d\Omega$$

$$\mathbf{B}_{\alpha\beta rs}=\frac{\Delta t^2}{2}\int_\Omega\left[\left(\mathbf{a}_{irq}\mathbf{a}_{jsq}+\frac{\mathbf{c}_{ijrs}}{\Delta t}\right)\Phi_{\alpha,i}\Phi_{\beta,j}\right]d\Omega$$

$$\mathbf{H}_{\alpha r}^n=\Delta t\int_\Omega\left[\Phi_{\alpha,i}\Phi_\beta\left(\mathbf{F}_{\beta ir}^n+\mathbf{G}_{\beta ir}^n\right)-\Phi_\alpha\Phi_\beta\mathbf{B}_{\beta r}^n-\frac{\Delta t^2}{2}\mathbf{a}_{irs}\Phi_{\alpha,i}\Phi_{\beta,j}\mathbf{F}_{\beta js}^n\right]d\Omega$$

$$\mathbf{N}_{\alpha r}^{n+1}=\frac{\Delta t^2}{2}\int_\Gamma\left(\mathbf{a}_{irq}\mathbf{a}_{jsq}+\frac{\mathbf{c}_{ijrs}}{\Delta t}\right)\dot{\Phi}_\alpha\,\Delta \mathbf{U}_{s,j}^{n+1}n_i d\Gamma$$

$$\mathbf{N}_{\alpha r}^n=-\int_\Gamma\left[\Delta t\,\dot{\Phi}_\alpha\left(\mathbf{F}_{ir}^n+\mathbf{G}_{ir}^n\right)-\frac{\Delta t^2}{2}\mathbf{a}_{irs}\dot{\Phi}_\alpha\,\mathbf{F}_{js,j}^n\right]n_i d\Gamma$$

It should be noted that the form (A14c) arises from (25) with $s_1 = s_3 = s_4 = b_j = 0$ and $s_2 = 1$, an algorithm similar to Hassan et al [13].

(c) Generalized Petrov-Galerkin (GPG)

The Generalized Petrov-Galerkin (GPG) method can be identified by setting $s_1 = s_2 = 1$, $s_3 = s_4 = 0$, $\mathbf{b}_i = \mathbf{c}_{ij} = \mathbf{d} = 0$, $\mathbf{Q}^n = 0$, $\mathbf{E}_i = \mathbf{a}_i$, and $\mathbf{E}_{ij} = \frac{1}{2}\Delta t^2\mathbf{a}_i\mathbf{a}_j$, so that (11) takes the form